REV.	BY & DATE	DESCRIPTION	CHECK	APPROVED & DATE
Prepared by Stefano Livi, Bruce Andrews, Dennis Haggerty, George Ho, and Barry Mauk	July 29, 2004	On-ground calibration report for the EPPS/EPS instrument.		

ADVISORY: This document has NOT been reviewed for export control and therefore may be subject to ITAR regulations or requirements.

PART NUMBER	SIZE	NEXT ASSEMBLY	QTY./NA	USED ON	EFFECTIVITY - END ITEM SER. NO.	WEIGHT

THE JOHNS HOPKINS UNIVERSITY
APPLIED PHYSICS LABORATORY
11100 JOHNS HOPKINS ROAD, LAUREL, MARYLAND 20723-6099

MESSENGER Energetic Particle Spectrometer (EPPS/EPS) Calibration Report

	FSCM NO.	SIZE	DRAWING NO.	REV.
	88898	A	7384-9471	A
	SCALE NONE	DO NOT SCALE PRINT		SHEET 1 OF 65

Table of Contents

1.0 INTRODUCTION

The Energetic Particle Spectrometer (EPS) is one of two sensors that comprise the Energetic Particle and Plasma Spectrometer (EPPS) package on the MESSENGER mission to Mercury. The other sensor is the Fast Ion Plasma Sensor (FIPS). EPS measures the high-energy components of the *in situ* electrons (> 15 keV) and ions (>5 keV/nucleon), while FIPS measures the low energy components of the ion distributions (< 20 keV / charge). Here we document the characterization and calibration of the EPS sensor, and describe future plans for finalizing the characterization of this sensor.

The MESSENGER Mission

The MErcury, Surface, Space ENvironment, GEochemistry, and Ranging (MESSENGER) mission will send the first spacecraft to orbit the planet Mercury. A miniaturized set of seven instruments, along with the spacecraft telecommunications system, provides the means of achieving the scientific objectives that motivate the mission. The payload includes a combined wide-angle and narrow-angle imaging system; γ-ray, neutron, and X-ray spectrometers for remote geochemical sensing; a vector magnetometer; a laser altimeter; a combined ultraviolet-visible and visible-infrared spectrometer to detect atmospheric species and map mineralogical absorption features; and an energetic particle and plasma spectrometer to characterize ionized species in the magnetosphere.

Launched in August 2004, MESSENGER will orbit Mercury for one Earth year following the following events:

Earth Flyby (1):	Jul 29, 2005
Venus Flybys (2):	Oct 23, 2006 and Jun 4, 2007
Mercury Flybys (3):	Jan 14, 2008, Oct 6, 2008, and Sep 29, 2009
Mercury Orbit Insertion:	Mar 18, 2011
Primary Science Orbit Start:	Mar 20, 2011

The EPPS Investigation

The Energetic Particle and Plasma Sensor (EPPS) Instrument Package consists of two separate physical packages, FIPS and EPS. Both sensors communicate to the MESSENGER spacecraft using the Event Processor Unit (EPU) computer located with the EPS sensor. Figure 1a, 1b, and 1c show the placement of the EPS and FIPS heads on the spacecraft and the EPS and FIPS fields-of-view (FOV). In these figure the sun is generally towards the –Y(s/c) axis and the imaging instruments point roughly in the +Z(s/c) direction. EPS has a 160° x 12° FOV with its center pointing along the +Y(s/c) axis away from the sun, one edge reaching within 10° of the +Z(s/c), often in the general direction of Mercury, and the other edge pointing within 10° of the –Z(s/c) axis, often in the "anti-Mercury" direction.

The overall EPPS instrument (including both EPS and FIPS) has a mass allocation of 3.07 kg and uses an allocated maximum (operational) power of 7.8 W (4.5 W of survival heater power).

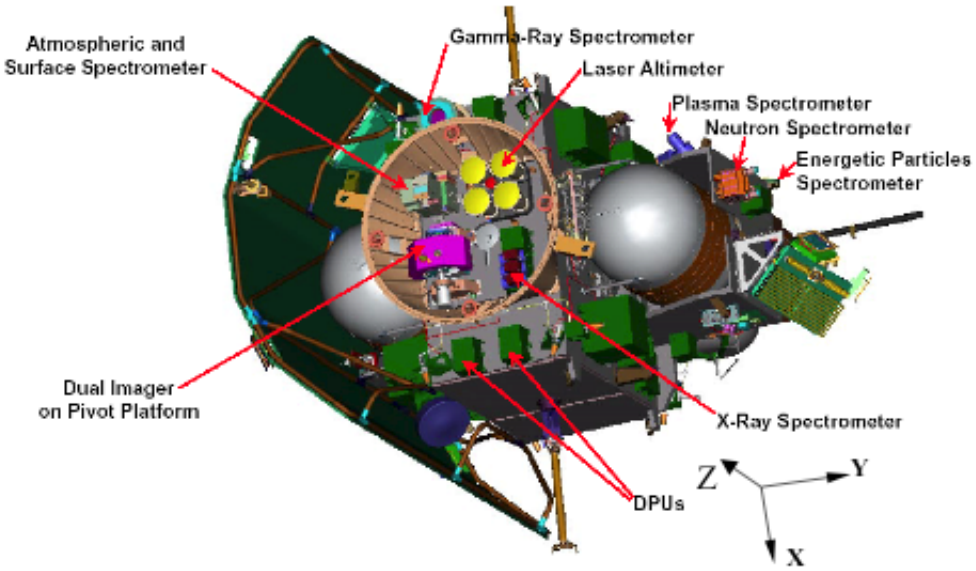

Figure 1a. Location of Energetic Particle Spectrometer on the Messenger spacecraft.

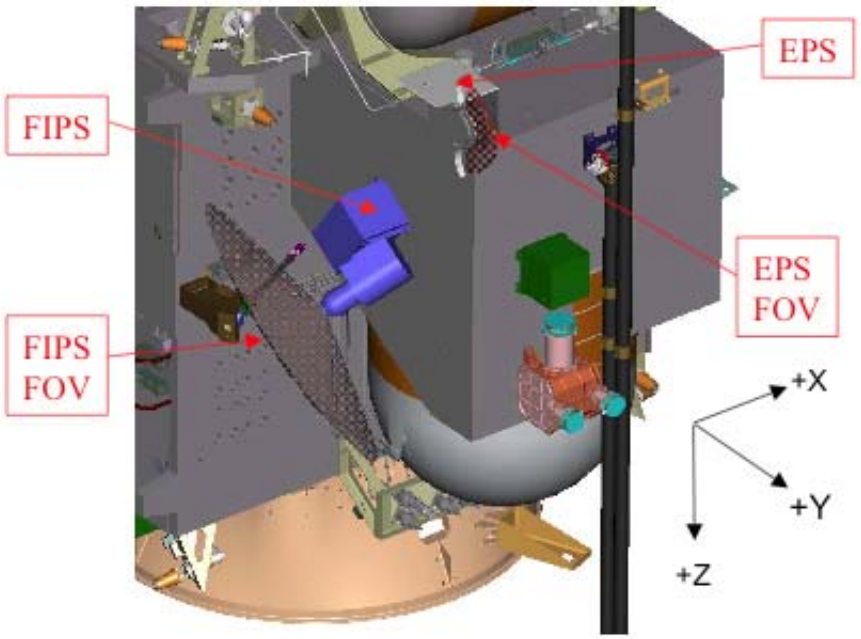

Figure 1b. Location of EPS and the EPS Field of View on the Messenger spacecraft.

FSCM NO.	SIZE	DRAWING NO.	REV.
88898	A	7384-9471	A
SCALE	DO NOT SCALE PRINT	SHEET 4 of 65	

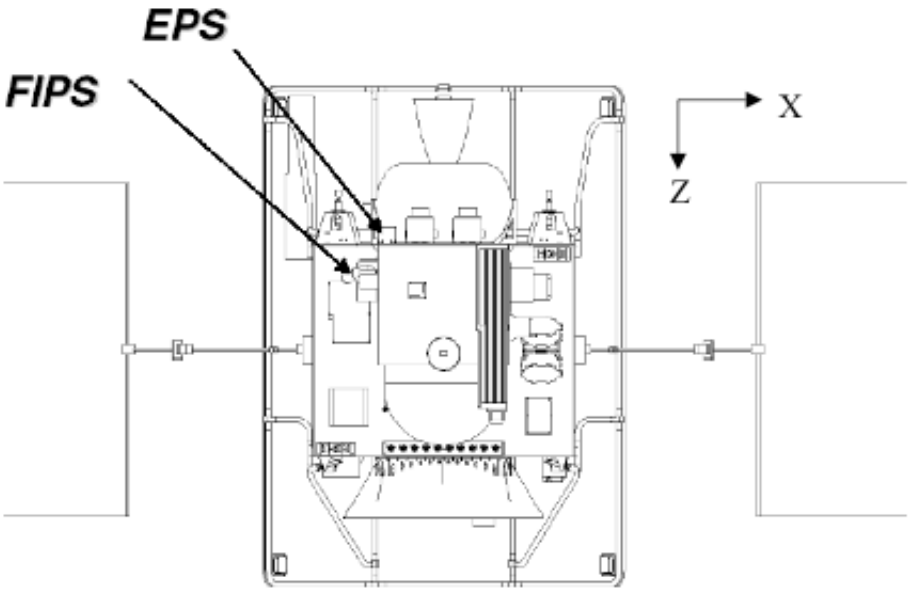

Figure 1c. Location of EPS and FIPS on the Messenger spacecraft.

In expanded form, the science goals of the EPPS instrument are:

1) To help determine Mercury's internal magnetic field by identifying some external current sources, identifying contaminating transients in the environment external to Mercury, and constraining the magnetic field topology by identifying field lines that connect to Mercury.
2) To characterize Mercury's exosphere neutrals by measuring the ionized products that arise from them and identifying ions accelerated by Mercury's magnetosphere.
3) To help determine the composition of the radar-reflective materials at Mercury's poles and other materials arising from Mercury's surface.
4) To determine the electrical properties of the crust/atmosphere/ space-environment interface.
5) To determine characteristics of the dynamics of the Mercurian magnetosphere and its relationship to external drivers and internal conditions.
6) To measure interplanetary plasma properties in cruise and in Mercury's vicinity.

These science goals tie directly back to the objectives listed in section 2.7 of the Program Level Requirements (PLR) document for the MESSENGER mission. The goals relevant to EPPS are to:

[3] Provide the capability to distinguish between solar and planetary sources of magnetospheric species.
[5] Provide in situ detection of H^+ or S^+ enrichment over polar regions.
[6] Provide the composition of magnetospheric ions and pickup ions in the solar wind from sputtered neutrals.

EPS contributes to these goals by measuring: i) spatial distributions of energetic ion pressures and other moments, ii) energetic ion and electron intensity versus time profiles for a broad range of energy and

species channels, iii) the major ionic species that comprise the ions intensities (H, He, CNO, heavies) iv) electron and ion angular distributions with respect to the magnetic field and the Mercury-Sun system, v) the positions and time variability of particle boundaries within Mercury magnetosphere, and vi) the energy and intensity depositions of particles onto Mercury's surface and exosphere.

The requirements are summarized in section 4.2.2.8 of the PLR which states "EPS shall be capable of measuring the elemental species H, He, CNO, and Fe, over an energy range from 10.0 keV/nuc to at least 3 MeV total energy and electrons from 25 keV to at least 500 keV."

Status of EPS Characterization and Calibration

The present (May 2004) characterization and calibration of EPS is less complete than is usual for an instrument that has been delivered to the spacecraft. The process of developing a ~1-2 kg (EPS is ~1.5 kg) instrument from a typically 5-10 kg class of instrument has been exceedingly challenging, and the instrument was delivered to the spacecraft with several known uncertainties in its performance. The largest problems included:

1) Total time-of-flight spread ~ 4-5 ns rather than the anticipated < 2 ns (the 4-5 ns is still sufficient to achieve the required clean separation of H, He, CNO, and Fe).
2) Efficiencies of double coincident signals (TOF plus E) much lower than expected (The efficiency of TOF alone – i.e. Low Energy Ions, is within the reasonable range of expectations).
3) Some cross talk (several percent) may occur in the classification of ion events within the FPGA ion species classifier (It appears that when two different ion species are present, H and O for example, some H ions may be assigned with the TOF of the O ion, and vice versa).

During the pre-delivery phase, the EPS team was faced with the quandary of either continuing to try to understand and fix the known performance problems or to just accept the performance as it is and to characterize it as best as we can. Thus, much work remains in characterizing the EPS instrument.

Since the instrument delivery, a flight-like engineering model has been built, and characterization of that unit is ongoing. We have achieved better understanding of the performance of the instrument and have are focusing in on the range of selectable high-voltage, reference-voltage, and discrimination values that optimize the performance of the EPS. For example, with knowledge gained with the engineering model we tuned the flight EPS during the Spacecraft Integration and Test and achieved a factor of 2 improvement in the TOF spread highlighted in item #1 above. Also, much higher double coincident efficiencies (and by inference TOF-only efficiencies) have been achieved with new parametric settings on the engineering model than yet tried on the flight model.

These engineering model characterizations will continue and the findings, in terms of parametric optimization of the EPS instrument, will be implemented and tested during the long periods of cruise (using the interplanetary energetic particle environment), and during planetary encounters of Earth and Venus, between the time of launch and the first flyby encounter of Mercury.

Table 1.1 Final EPS Engineering Parameters and Assessment against requirements

Parameter	CSR/PLR Requirement / Expectation	Measured or derived from Measurements	Comments (PLR takes precedent over CSR)
Engineering Parameters			
Mass	1.3 kg (including FIPS)	EPS only: 1.5 kg	Includes cable to FIPS
Power Average	2 W (including FIPS)	EPS only: 4.8W primary	Includes Converter losses for FIPS: FIPS uses and additional 2 W
Power Peak	same	same	Additional power needed one time to deploy cover
Data Rates: Average	80/2 bps	91 bps	With DPU Compression
Data Rates: Peak		~500 bps	With DPU Compression
Size	"Hockey Puck"	15.55 x 12.98 x 11.25 cm	Includes mounting tabs / structures
Performance Parameters			
Geometric Factor	0.1 cm^2.s	0.0074 cm^2 sr	Calculated: PDR Expectation: 0.01. Decrease driven by electron scattering issues
Ion Energy Range	10 keV/n to 3 MeV	10 keV/n to ~3 MeV	Lowest energies with TOF-only, as expected
Electron Energies	25 to 500 keV	25 to 500 keV	> 170 keV based on electron SSD response to Radiation Source.
Species	H, He, CNO, Fe, electrons	H, He, CNO, electrons	Fe measurement expected by extrapolation of measurements
Field-of-View	160° x 12°	160° x 12°	
Angular Resolution	160°/6	~30 deg.	No explicit requirements
TOF Range	0-200 ns, ±200 ps	10-200 ns, ±1500 ps	Sufficient for required mass discr.
Integration period	Fixed: 36 s	0.5 – 300 s	Programmable

Assessment of the EPS Instrument Performance Against Requirements.

As described in the previous minor section, the calibration and characterization of the EPS instrument is ongoing and will continue long after the launch of the MESSENGER Spacecraft. However, we know enough about the EPS performance to compare what we know about it against the MESSENGER Program Level Requirements and the MESSENGER Concept Study Report requirements for EPS. The high level characteristics of EPS as compared to requirements are shown in Table 1.1. The present understanding of the performance of the EPS instrument is provided in Table 6.1. The major deviation

from performance expectations (not requirements) is the uncertainty regarding the efficiency of the triple coincidence TOF versus Energy ion measurements. Should the poor efficiency performance on triple coincidence ion measurements persist, despite indications with an engineering model that efficiencies will rise once the instrument is optimized after launch (with various discrimination and voltage settings), the EPS requirements are still met. Fast ion measurements will be made with the double-coincident TOF-only ion measurement. Composition measurement requirements will be achieved but over longer integration times than anticipated at the time of the MESSENGER Concept Study Report.

2.0 EPS INSTRUMENT DESCRIPTION

EPS Sensor Description

The Energetic Particle Spectrometer (EPS) is a miniature Time-of-Flight (TOF) versus Energy (E) spectrometer that measures ions and electrons over a broad range of energies and pitch angles. Directional ion composition and energy spectra are measured for H to Fe from >5 keV/nucleon to ~3 MeV total energy. Directional electron energy spectra are measured from 25 keV to 0.6 MeV. A picture of the EPS instrument on the bench is shown in Figure 2 without the thermal radiator that partially obscures the view of EPS in Figure 1.

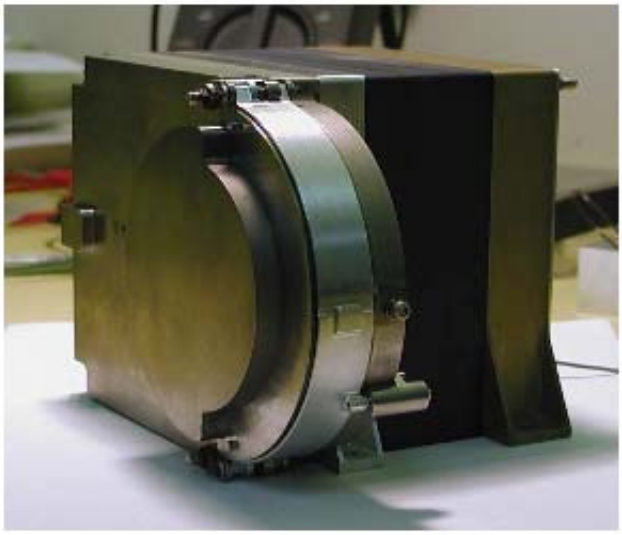

Figure 2. EPS Sensor

Heritage. EPS was designed and manufactured at the Johns Hopkins University Applied Physics Laboratory (JHU/APL) based on technologies developed for many previous missions. The TOF vs. E technique was first implemented for energetic ions with the MEPA instrument on the Ampte Mission. It has since been flown on Galileo Energetic Particle Detector (EPD), and Geotail Energetic Particle Ion Composition (EPIC) for measuring energetic ions, and on Cassini Magnetospheric Imaging Instrument (MIMI) and Imager for Magnetopause-to-Aurora Global Exploration (IMAGE) High-Energy Neutral Atoms (HENA) instrument for measuring energetic neutral atoms. For previous energetic ion

applications, the directionality of the ions was determined by means of mechanical and spacecraft rotations of well-collimated, single conical view sensors. The new element on MESSENGER EPS is that multiple simultaneous views (6) are obtained using a single time-of-flight chamber [McNutt et al., 1996; Andrews et al., 1998].

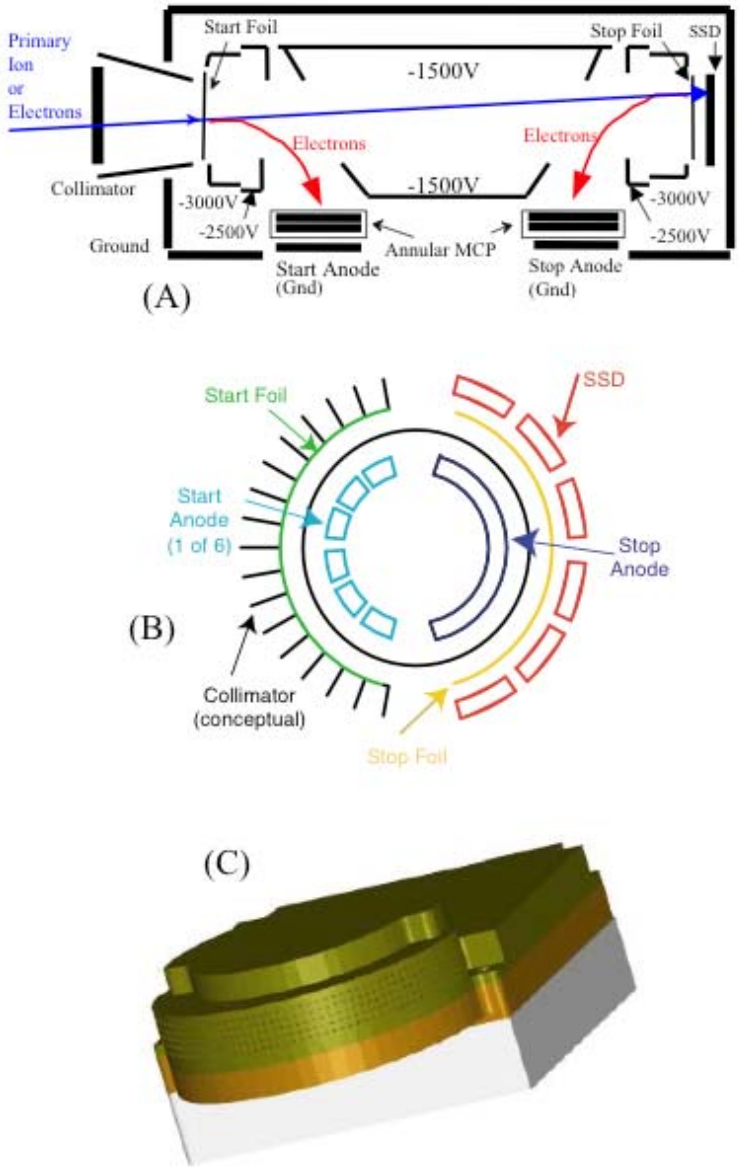

Figure 3. How EPS operates.

FSCM NO.	SIZE	DRAWING NO.	REV.
88898	A	7384-9471	A
SCALE	DO NOT SCALE PRINT	SHEET 9 of 65	

Time-of-Flight Operation. Figure 3 shows how EPS operates. In Figure 3a, ions (blue) enter the collimator on the left, penetrate a "start" foil, pass thought the time-of-flight drift chamber, penetrate a "stop" foil, and then imbed themselves within the solid-state-detectors (SSDs) on the right. As the ions pass through the start and stop foils, secondary electrons are generated (red). The secondary electrons are electrostatically steered onto different sections of a circular Microchannel Plate (MCP). Segmented anodes collect the MCP-amplified signals from the different sections of the MCP. A JHU/APL developed time-of-flight (TOF) application-specific integrated circuit (ASIC) uses the start and stop signals to derive a TOF value in the ~1 to 200 nsec range. A RTX-2010 microprocessor uses the TOF value and the total energy E value from the solid-state detector (SSD) to identify the elemental mass species M and the total ion energy E. Such double-coincident (TOF plus E) events are called "High Energy Ions". That TOF versus E information can be used to so sort the incoming ions was proven on previous missions such as the Galileo EPD instrument, with data presented in Figure 4. Ions that generate a TOF signal but do not generate a SSD signal are also processed as "Low Energy Ions". With such low-energy ions, crude compositional information is retrieved using the TOF value and the MCP pulse height (PH). The pulse height is discriminated by EPS with 2 MCP discrimination levels over and above the noise-threshold discriminator. That TOF versus PH can crudely discriminate between heavy and light species was demonstrated with the IMAGE HENA instrument (Figure 5). The TOF performance depends on the time dispersion associated with the secondary electron trajectories plus the dispersion introduced by the electronic signal processing. Simulations of that dispersion are shown in a later section.

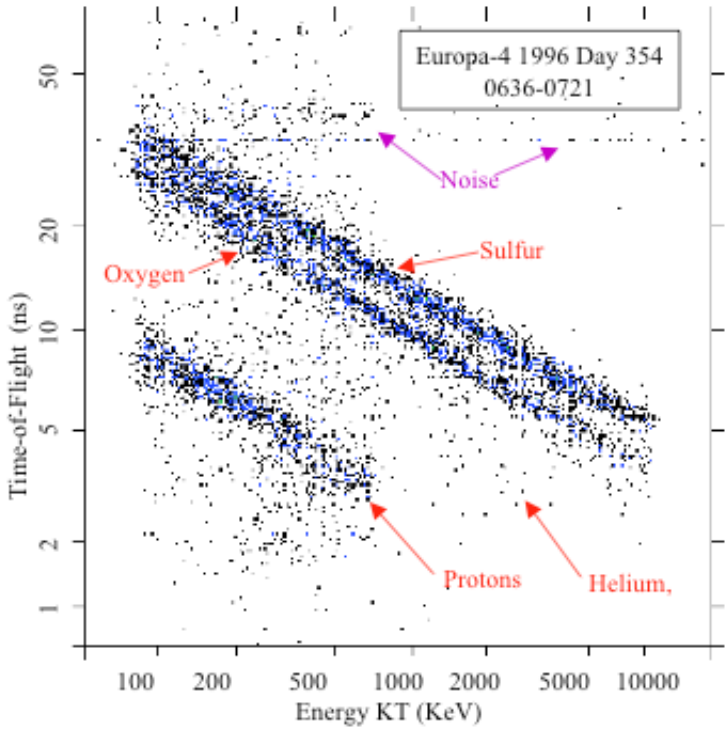

Figure 4. Expected EPS Time-of-flight versus energy performance as illustrated using Galileo EPD data

FSCM NO.	SIZE	DRAWING NO.	REV.
88898	A	7384-9471	A
SCALE	DO NOT SCALE PRINT	SHEET 10 of 65	

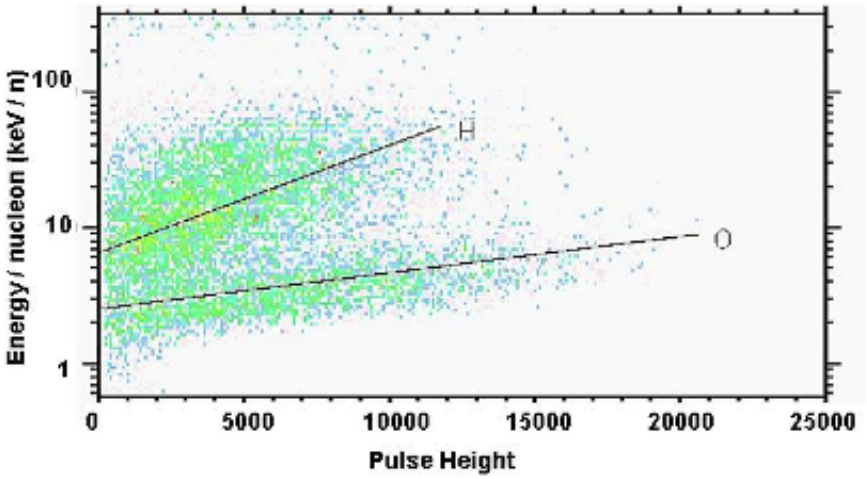

Figure 5. expected EPS Time-of-flight versus MCP pulse-height performance as illustrated using Image HENA data

Foils and Materials. The performance of EPS depends on the materials through which the particles must pass. Such materials degrade particle energy and scatter particles in angle. The start foil consists of 500 Å of polyamide covered on both surfaces with 50 Å of aluminum to ensure conductivity of the outer layer of the foil and enhance rejection of ultraviolet light, particularly Ly-α. The stop foil also consists of 500 Å of polyamide, but it is additionally covered by 100 Å of palladium to reduce further light (both visible and UV) transmission toward the SSDs. The foils are mounted on ~90% transmittance stainless steel grids. Dead-layers on the SSDs are of order 500 Å. The cylindrical foil holder has an inner radius from the center of the sensor of ~2.88 cm. The entrance and exit apertures within the foil holders have a height of 0.615 cm. The entrance and exit foils each comprise two separate foils, and so the foil holder has a 0.127 cm blockage at just the very center of the sensor FOV (which translates into ~5°). Some views of the mechanical configuration of EPS are provided in Appendix 12.

Directionality. Figure 3b shows that from the top, the EPS sensor volume has cylindrical symmetry. The multi-hole collimator (Figure 3c; the collimator in Figure 3b is notional only) ideally maps particles arriving from one specific direction on the left uniquely past just one of the 6 start anodes on the left and uniquely onto just one of the 6 SSDs on the right. The direction, from which the ion arrives, in one angular dimension, is therefore determined by which SSD is activated (for "high-energy ions") or which start anode is activated (for "low-energy ions"). Because of a compromise to achieve the highest level of sensitivity (high geometric factor, see below) the collimator was opened up somewhat so that the angular response has side lobes at the several-percent level. Deconvolution of the collimator response will therefore be required to derive angular distributions with the highest fidelity.

Solid-State-Detectors. Each of the 6 SSDs has four pixels, two dedicated to the ion measurements described above, and two to electron measurements (Figure 6a), for a total of 24 SSD elements. For each species (ions or electrons) on each of the SSDs there is both a large area pixel (40 mm^2) and a small area pixel (2 mm^2). These 2 pixels allow for flexibility in the geometric factors (hence sensitivity and dynamic range) of the sensor. At any one time, 12 of the 24 elements are used. One may choose any

combination of : i) large-ions / large-electrons, ii) large-ions / small-electrons, iii) small-ions / large-electrons, or iv) small-ions / small-electrons (for all 6 SSD's simultaneously). Two views of the SSD mounting structure are shown in Figure 6b. The surfaces of the SSD are positioned ~3 mm behind the stop-foil mounting structure.

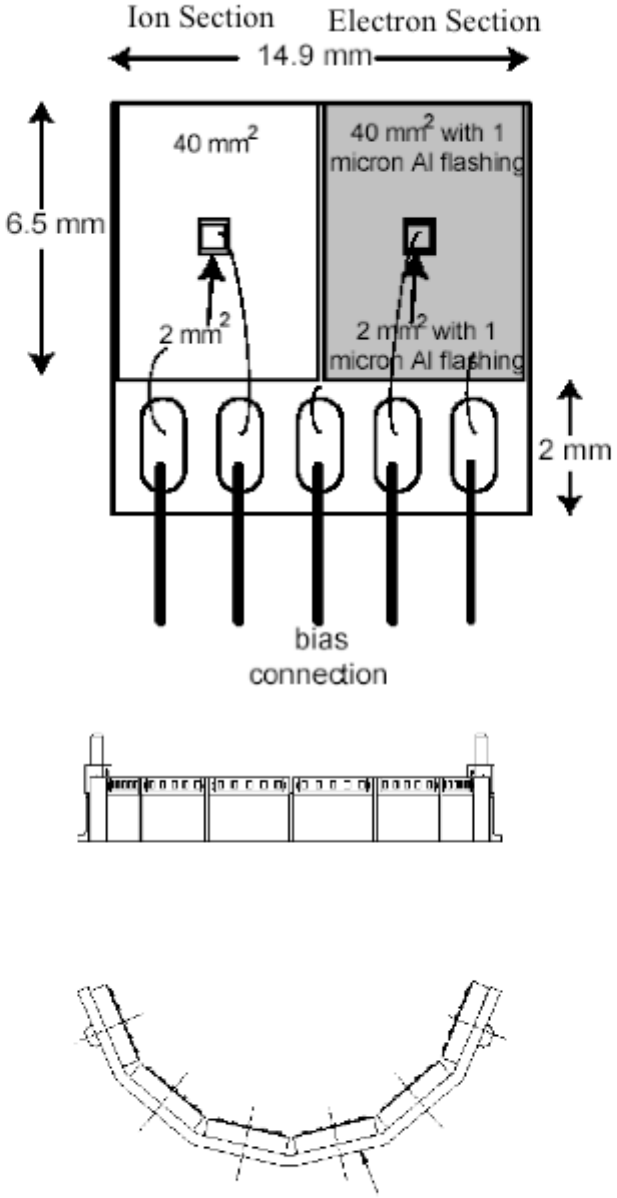

Figure 6. Solid State Detector configuration on EPS.

Electron Measurements. A thin layer (flashing) of 1 μm of Aluminum covers the SSD elements dedicated to electron detection. This dead layer stops protons with energy less then 200 keV; while electrons loose less then 10 keV energy by the interaction with this additional layer. Electrons are identified in EPS by the presence of an energy signal in one of the electron SSD elements and by the absence of start and stop pulses. Energetic electrons have low efficiency for production of secondary electrons when passing through thin foils (< 1%). Under such conditions, a signal of 50keV in the electron detector can be generated either by a ~250 keV proton that did not generate either a start or a stop pulse (with a probability of perhaps < 25%), or by a 60 keV electron. The TOF vs E and TOF vs. PH spectra collected in the adjacent ion SSD element (without flashing) are used during ground data analysis for checking and correcting for the proton contamination within the electron SSDs

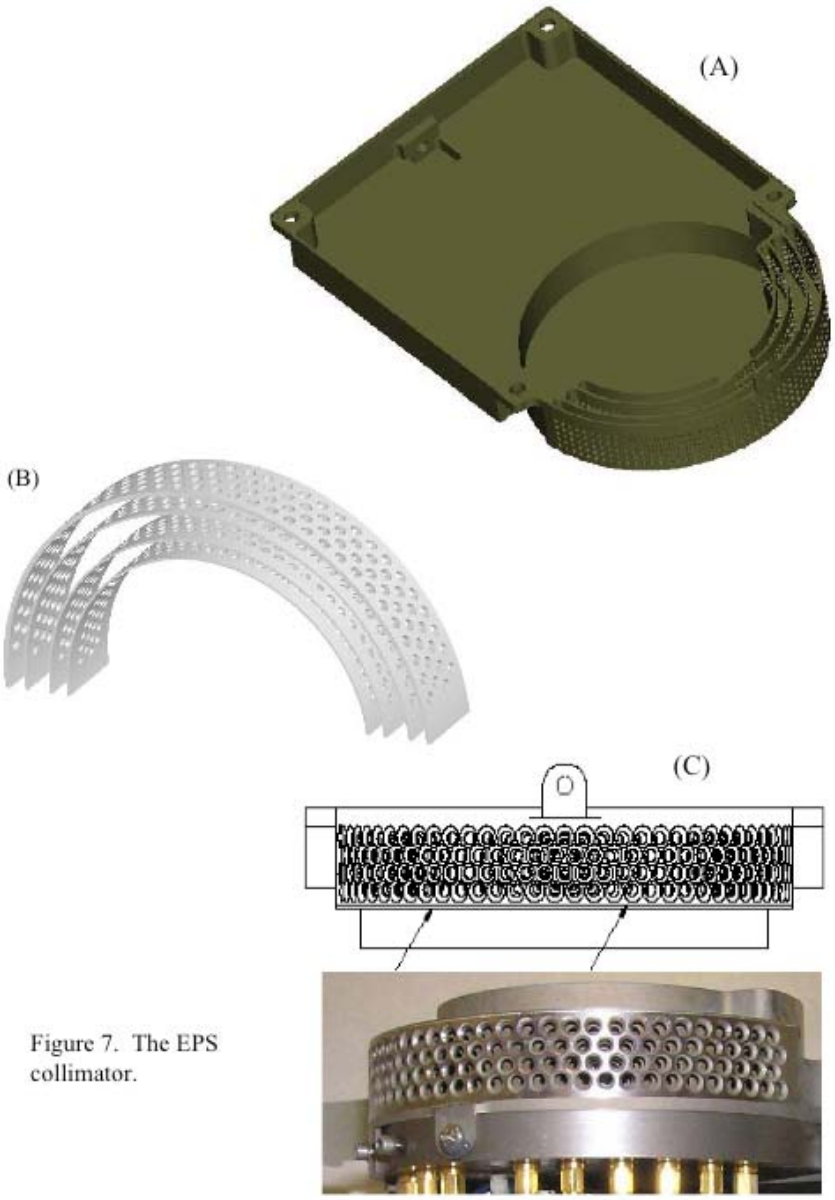

Figure 7. The EPS collimator.

FSCM NO.	SIZE	DRAWING NO.	REV.
88898	A	7384-9471	A
SCALE	DO NOT SCALE PRINT	SHEET 13 of 65	

Collimator. The EPS collimator consists of 4 concentric, thin (20 mils) titanium sheets perforated with a regular pattern of holes (Figure 7). The holes are drilled so that, if one imagines straws passing through each of the set of 4 holes that pass through the 4 concentric sheets, all of the straws would focus onto a single point right at the center of the cylindrical structure of the sensor half way between the start and stop foils. That is, even while the walls of the collimator have cylindrical symmetry, the hole-patterns themselves have spherical symmetry. Even the sizes of the holes have spherical symmetry; that is, the sizes of the holes in the 4 concentric titanium sheets are proportional to the distance from the focal point in the center of the sensor. This design has two advantages over commonly used collimators: i) the geometric factor for particles striking the front foil of the sensor is essentially the same as the geometric factor of the entire sensor (thus minimizing the accidental rates that arise from high counting from the start foil), and ii) the primary particles are kept well away from surfaces within the sensor that can scatter particles. Figure 7c shows a front-side view of the collimator, as it would appear to a detectable particle approaching the entrance aperture. The inner radii of the 4 cylindrical sheets that constitute the collimator are: 4.50, 4.12, 3.58, and 3.20 cm. The holes in the sheets have diameters 2.34, 2.24, 1.66, and 1.68 mm and are arrayed in a hexagonal pattern of 4 rows (Figure 7c). The centers of the holes in the outermost and innermost rows view 3.83° and 1.92° away from central plane. There are 33 holes per row spanning the ~160° FOV. Each set of 4 aligned holes has an absolute maximum geometric full-width acceptance cone of 8.8°, and so that 2 x 2.38° + 8.8° = 13.56° is the absolute full-width of the viewing fan. The full width at half maximum is roughly 12.2°.

If the holes within the collimator walls are relatively small, then the mapping of particles that come from a singe direction (and illuminate the entire instrument) to a single position at the plane of the solid state detectors is well behaved. As mentioned in a previous section, the holes in the EPS collimator are larger than those that would be optimum for angular response in order to achieve greater sensitivity. Thus, the angular response has side lobes, as described in a later section.

Electron / ion fields of view and detector numberings. The nominal total field-of-view (FOV) of EPS is 160° x 12°. Because the electron and ion SSD's are side-by-side, the total electron or ion FOV in the long dimension is about 1/12 smaller (~13° smaller) or about 147°. And, the centers of the ion and electron FOV's are shifted with respect to each other by ~13°. In Figure 1, let us define two angles: "alpha" is the angle from the +Y(s/c) axis and within the Y(s/c)-Z(s/c) plane (with "plus" angles viewing towards the +Z(s/c) axis); "beta" is the angle for rotations away from the Y(s/c)-Z(s/c) plane. With these definitions, the total FOV of EPS is roughly: (-80° < alpha < +80°) and (-6° < beta < +6°). The ion FOV is (-67° < alpha < +80°) and (-6° < beta < +6°). The electron FOV is (-80° < alpha < +67°) and (-6° < beta < +6°).

With the ion and electron segments, there are a total of 12 SSD elements active at any one time. The numbering scheme for these detector elements ranges between 0 and 11, with the even SSD elements corresponding to electrons and the odd SSD elements corresponding to ions. The numbering does not change with the selection of large or small detectors for either ions or electrons. The complete specification of an EPS detector element would be, for example: "SSD element 3 small". In Figure 1, the "0" detector (an electron detector) is the one that looks most closely aligned with the –Z(s/c) axis.

The numbering of the TOF Start-Anodes ranges between 0 and 5. An ion or electron that passes right over Start-Anode "0" (only the ion "stimulates" this start anode) strikes either SSD 10 or SSD 11. Thus,

the Start-Anodes 5, 4, 3, 2, 1, and 0 map to SSD's (0, 1), (2, 3), (4, 5), (6, 7), (8, 9), and (10, 11), respectively.

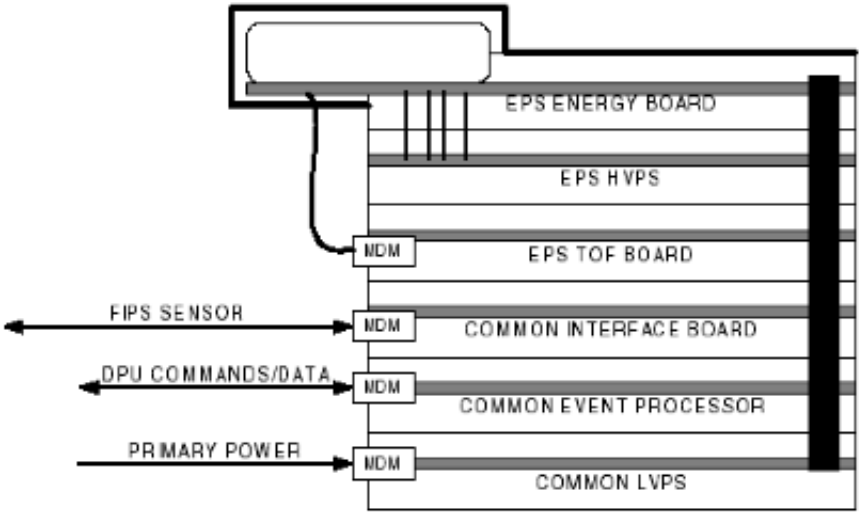

Figure 8. EPS Board layout configuration

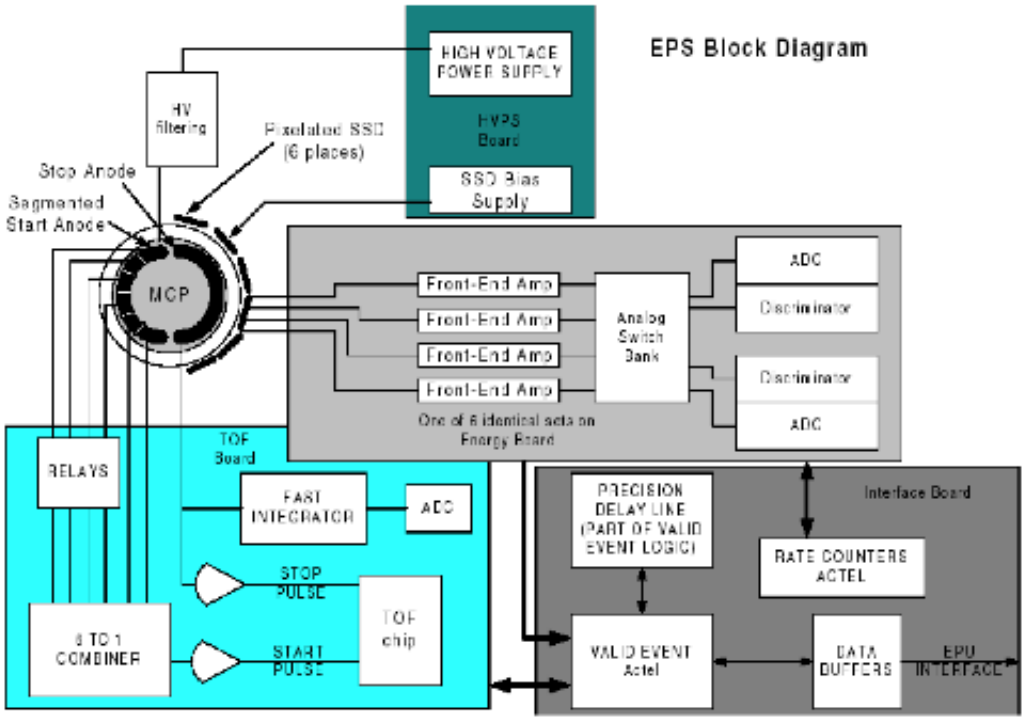

Figure 9. EPS Block diagram.

EPS Electronics Description

The layout of the EPS electronic boards is shown in Figure 8 and an EPS Block diagram is shown in Figure 9.

SSD Detector Pulse Conditioning and Measurement. The SSD charge amplifier used (the "front end amp in Figure 10) is an Amptek A250F followed by a 2.4 microsec shaping stage utilizing an AD8032. An A/D converter accepts the shaped pulses with a maximum input of 2.5V. The shaping circuit also outputs a fast timing pulse that is used for "time-to-peak" digitization purposes. A PHA SSD pulse amplitude is obtained both at the time that the fast pulse is first detected (the so-called baseline measurement), and at the time of the peak in the shaped pulse. Both the baseline and the peak amplitude are captured within the PHA event packets. The energy measurement is based on the difference between the peak and the baseline measurement (unless a commanded choice is made to use only the peak value). Only twelve of the 24 A250F's are powered at any given time based on the setting of the "analog switch bank" (either the large pixel or the small pixel preamps). The conversion between SSD electronic energy and PHA bin number is: Energy (keV) = 0.57387 * bin#.

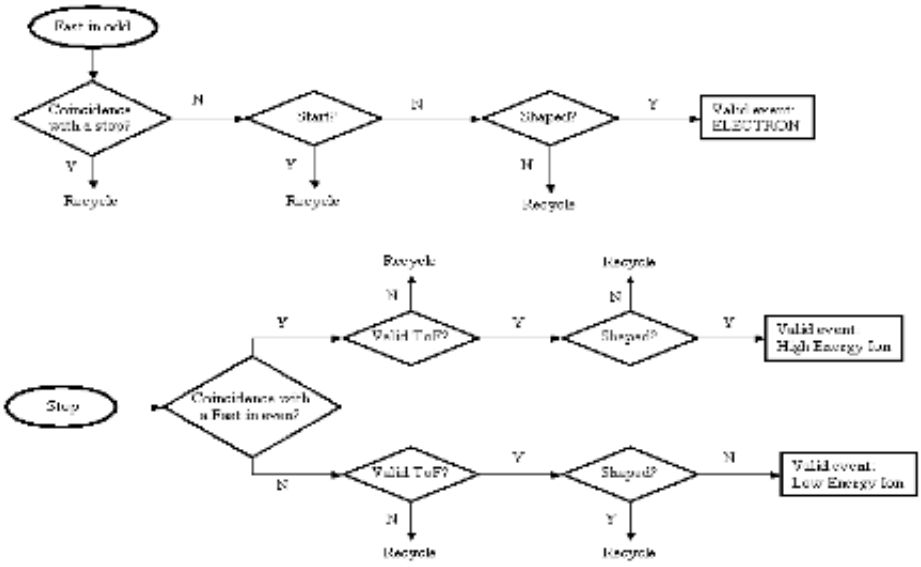

Figure 10. EPS valid event logic.

SSD Detector Thresholds. Eight D/A converters are used to set the threshold of groups of three discriminators. The DAC grouping is shown below. An event that is registered within the SSD is used to generate two separate pulses, a fast pulse used for timing (ergo the "timing" discriminator) and a slow pulse used for pulse-height analysis (the "shaped" discriminator). The "timing" referred to here should not be confused with time-of-flight measurement.

1. timing discriminator (Electron channels 0,2,4)
2. shaped discriminators (Electron channels 0,2,4)
3. timing discriminator (Ion channels 1,3,5)
4. shaped discriminators (Ion channels 1,3,5)
5. timing discriminator (Electron channels 6,8,10)
6. shaped discriminators (Electron channels 6,8,10)
7. timing discriminator (Ion channels7,9,11)
8. shaped discriminators (Ion channels 7,9,11)

These settings are communicated to the ground as part of the housekeeping data carried with the EPS high priority, as shown in Table 2 of Appendix 4.

Detector Channel Control. All 12 detector channels have fully independent circuitry that feeds a common FPGA-based control circuit. By masking its discriminator firings via a software-programmable register, a noisy channel may be ignored.

Time-of-Flight System. Micro-channel plates (MCPs) are used as time-of-flight start and stop pulse detectors. Seven anodes (six start and one stop) go directly to the Time-of-Flight board via coax cables. Each of the six start anodes is split into two isolated signal paths:

1. Input to a discriminator (with adjustable threshold) and used to identify which anode fired
2. Recombined with other start anode signals, amplified and used as start pulse for the TOF chip via a Constant Fraction Discriminator (CFD)

The stop anode signal is also split into two isolated signals:

1. One signal forms the stop pulse for the TOF chip via a CFD
2. The other signal is fed to two level discriminators which are used to indicated whether the particle was “light” (H or He), “medium”, or “heavy” (C, N, O, Fe)

The threshold settings are communicated to the ground as part of the housekeeping data carried with the EPS high priority, as shown in Table 2 of Appendix 4. The time-of-flight (TOF) value is digitized into discrete bins with the conversion: TOF (ns) = 0.16276 * bin#.

Rate Counters. A total of 35 rate counters are implemented in a field-programmable gate array (FPGA). All counters are 16-bit counters, except START, STOP and VALID TOF, which are 24 bits deep. These counters are read out directly from the FPGA in response to 38 unique address-decoded read cycles from the processor. In addition, the RTX2010 Event Processor generates 7 additional counters. The hardware and software counters are documented in Appendices 1 and 2.

Event Logic. During normal operation, EPS generates 3 different data products, “Electron Data”, “Low Energy Ion Data (LEID)” and “High Energy Ion Data (HEID).” A schematic diagram of the logic producing valid events is provided in Figure 10. EPS can be put into a mode (the diagnostic mode) where, instead of generating LEID and HEID it generates ion spectra based solely on the ion SSD

energy events (TOF and PH are ignored). Here the "SSD Ion Data" is generated in a fashion exactly parallel to the process that generates the Electron Data.

It is possible to command a decimation of the electron throughput in order to prevent the electron rates from overwhelming the ion rates within the Event Processing Unit.

Event Packets. The physical information in a valid event is stored in a block of words (16 bit) called event packets. These events are stored by the FPGA controller into FIFO and are read out by the RTX2010 Event Processor Unit. Four different event packets have been defined: 1) Electron Packets, 2) High Energy Ion Packets, 3) Low Energy Ion Packets, and 4) Diagnostic Packets. The information contained in these event packets, as package for telemetry to the ground for selected events, is shown in Appendix 7.

Software Event Processing. The EPPS software obtains event data through two separate FIFOs, one for EPS and one for FIPS. Event packets consist of a number of event words. The total number of words in a packet depends on the type of event, as described in the last subsection. The first word within each event packet contains a synchronization pattern and an ID that specifies the event type. The synchronization pattern is used to detect the beginning of a new packet.

The acceptable throughput for EPS event processing is of order 5 kHz. During high counting situations the processed events are designed to "poll" the incoming events and thus maintain the correct distribution of ion energies, species, and directionality; and separately, the correct distribution of electron energies and directionality. The correct particle intensities are derived by ratioing the appropriate hardware counters with the appropriate software counters. Note that when the rate of incoming particles exceeds the capabilities of even the hardware, such simple ratioing does not suffice. Part of the characterization and calibration activities is to determine the so-called "Rate-versus-Rate" corrections (so called R-R corrections) associated with extremely high counting situations.

One way that the EPU processes event packets is to generate spectra or histograms for the various event types by using lookup tables to determine the corresponding bin within each spectrum to increment. These lookup tables are accessed based on some combination of the energy, time-of-flight and/or mass-to-charge ratio depending on whether the particle is from the EPS or FIPS system. For example, with EPS the TOF versus E space shown in Figure 4 is, for each of the 6 view directions, divided into 22 different histogram bins to generate the EPS High Energy Ion data. Also with EPS, the TOF versus Pulse Height space shown in Figure 5 is divided into 16 different bins to generate the Low Energy Ion data. The bins to be incremented within the electron spectra are determined based on the electron event energies. Eight different energy ranges are used. The channel definitions for Electrons, Low Energy Ions, High Energy Ions, and Diagnostic Mode Ions are provided in Appendix 8.

The EPPS instrument software system can also be commanded into a "test mode" in which it accepts commands from and outputs selected science and status information through an RS-422 test port. A test-port may also be employed to supply a source of simulated event data for use in instrument checkout.

The accumulation, formatting and reporting of EPS event and housekeeping data are synchronized to two different time intervals. These are referred to as the N1 and N2 time intervals. The N1 time interval is nominally 300 seconds and is an integral multiple of the N2 time interval. The N2 time interval has a nominal value of 30 seconds. Either or both of the intervals can be changed via command. However, the value for N1 should always be a multiple of the N2 value. (If N1 is not a multiple of N2, the medium priority data becomes garbled and uninterruptible). Among the data collected at these intervals are the 35 hardware rate counter registers. To prevent these registers from overflowing, each of the intervals N1 and N2 is subdivided into 10 equal-length subintervals. Thus the basic integration period corresponds to N2/10 seconds. The EPS-event first-in-first-out (FIFO) is flushed at the conclusion of each N2/10 interval to keep the events that occur during different time intervals separate.

Hence all data products for the EPS subsystem are collected at the N2/10 second rate. Values that are reported every N2 seconds are produced by summing the 10 consecutive N2/10 samples. Values that are reported every N1 seconds are produced by summing over as many N2/10 subintervals as there are in the N1-second time period.

EPS Telemetry. The High-Priority, Medium-Priority and Low-Priority data formats for EPS are documented in Appendices 4, 5, and 6. High-Priority and Low-Priority data is collected at a cadence of N1 (last subsection; often 300s). Medium-Priority data is collected at a cadence of N2 (30s or less). The Pulse-Height-Analysis-event formats imbedded in these data products are documented in Appendix 7. Appendices 4 and 5 also document in red the changes that result when EPS is put into the Diagnostic Mode for measuring Ion Spectra (and Electron Spectra) while ignoring the TOF system. Finally, the status of the EPPS instrument, including EPS is communicated through a separate EPPS Status Packet as documented in Appendix 3.

Pulse-Height Analysis Priority Scheme.

In order to prevent the most common particle species from overwhelming the Pulse-Height-Analysis (PHA) events that are sent to the ground, a rotating priority scheme is used for selecting species groups. The priority scheme is documented in the EPPS Flight Software Specification Document (MESSENGER Document JHU/APL 7389-9041).

3.0 SCOPE OF CHARACTERIZATION AND CALIBRATION

EPS measurements are intended to generate the information needed to derive the charged ion and electron differential intensities (**I** [cm^{-2} sr^{-1} s^{-1} keV^{-1}]) and phase space densities (**PSD**[s^3 cm^{-6}]). The significance of **I** and **PSD** are that, for many particle transport processes within planetary magnetospheres and interplanetary space, they satisfy the collision-less Boltzmann equation, derived from Liouville's Theorem for collision-less transport, for energy preserving, and for non-energy preserving processes, respectively. Our purpose here is to develop the quantitative procedures for converting the count rates (**R**[counts s^{-1}]) reported by EPS in the many predefined channels described in preceding sections, or in channels defined on the ground using the pulse-height-analysis (PHA) data, into estimates of **I** and **PSD** for the various defined ranges of energies, particle species, and arrival angles. We begin by defining terms.

Flux, differential intensity and phase space density

The rate **R**[particles/s] that traverse an area A can be given by the Flux **F** [cm^{-2} s^{-1}] with:

$$\mathbf{R} = A * \mathbf{F} \quad (1)$$

or by the intensity **i** [cm^2 s^{-1} sr^{-1}]

$$\mathbf{R} = A * \int \mathbf{i} \cos(\hat{u})\, d\Omega \quad (2)$$

where Ω is solid angle and $\hat{u}$ is the angle to the area normal.

Often used is the quantity differential intensity **I** [cm^2 s^{-1} sr^{-1} keV^{-1}], defined as the number of particles of a given species S with energy between E and E+ΔE that traverse the area A during the time t, where

$$\mathbf{R}(S, E) = \mathbf{I}(S, E) * A * \Delta\Omega * \Delta E \quad (3)$$

In three dimensions, with θ being the polar angle and ϕ the azimuthal angle of a polar reference system:

$$d^3\mathbf{R}(S, E,\theta,\phi) = \mathbf{I}(S, E, \theta, \phi) * A(\theta, \phi) \cos(\hat{u}) * t * dE \cos\theta\, d\theta\, d\phi \quad (4)$$

where we note that the area A and the unit vector $\hat{u}$ pointing normal to A are both functions of θ and ϕ.

Note that for non-relativistic energies, **I**(S, E, θ, ϕ) is related to the phase space density **PSD** (number of particles in the configuration space element d^3R and with velocity between v and v+ d^3v) by the simple relationship

$$\mathbf{PSD}[s^3\ cm^{-6}] = \mathbf{I}[cm^2\ s^{-1}\ sr^{-1}\ keV^{-1}] * m/v^2 \quad (5)$$

For relativistic energies, the phase space density (identified with lower case letters here: **psd**) is defined in terms of particle momentum **p** (**psd**[s^3 cm^{-6} kgm^{-3}]), and the relationship to differential intensity **I** is:

$$\mathbf{psd}[s^3\ cm^{-6}\ kgm^{-3}] = \mathbf{I}[cm^2\ s^{-1}\ sr^{-1}\ keV^{-1}] / \mathbf{p}^2 \quad (6)$$

Definition of sensor transfer function and geometric factor

Using (4), the rate **R**[particles/s] of particles of species S, in the energy band ΔE around mean energy E, angular band $\Delta\theta$ around mean polar direction θ, and angular band $\Delta\phi$ around the mean azimuthal direction ϕ, measured by the instrument can be expressed as:

$$\mathbf{R}(S, E) = \int_{\Delta E}\int_{d\theta}\int_{d\phi} \mathbf{I}(S, E, \theta, \phi) * A(\theta, \phi) \cos(\hat{u}) * dE \cos(\theta)\, d\theta\, d\phi \quad (7)$$

One may take the kernel approach to relating **R** to **I** by allowing **I**(S, E, θ, ϕ) to be a Dirac δ-function (mono-energetic, infinitely narrow beam). Then:

$$d\mathbf{R}(S, E, \theta, \phi) = d\mathbf{I}(S, E, \theta, \phi) * \mathbf{T}(S, E, \theta, \phi) \quad (8)$$

where **G**(S, E, θ, ϕ) [cm^2 sr keV] is the kernel, also known as the "transfer function" of the instrument. Then:

$$\mathbf{R}(S,E) = \int_{\Delta E} \int_{d\theta} \int_{d\phi} \mathbf{I}(S, E, \theta, \phi) * \mathbf{T}(S, E, \theta, \phi) \cos(\theta) d\theta \, d\phi \quad (9)$$

It is typical for the first estimate to assume that the particle intensities are constant over the energy-species-angle bandwidths of any one channel. The estimated intensity $\mathbf{I}_{kj}$ associated with a specific detector **k**, which at a specific time views a range of angles centered in a specific direction (θ_k, ϕ_k), and which is associated with a specific energy channel **j**, which measures particle species $\mathbf{S}_j$ over an energy range that stretches from E_j to $E_j + \Delta E_j$, is given by equation (9) as:

$$\mathbf{R}_{kj} = \int_{\Delta Ej} R_k(S_j, E_j)\, dE = \int_{\Delta Ej} \mathbf{I}_k(S_j, E) * \mathbf{T}(S_j, E))\, dE \sim \langle \mathbf{T}_{kj} \rangle \mathbf{I}_k(S_j, E_j)\, \Delta E_{kj} \quad (10)$$

where $\mathbf{R}_{kj}$ is the channel count rate and where $\langle \mathbf{T}_{jk} \rangle$ is called here the Transfer Factor $\mathbf{H}_{kj}$. It is convenient to separate $\mathbf{H}_{kj}$ into a counting efficiency "$\boldsymbol{\varepsilon}_{kj}$" and a factor that relates strictly to geometry, the so-called Geometric Factor $\mathbf{G}_{kj}$. That is:

$$\mathbf{I}_k(S_j, E_j) \sim \mathbf{R}_{kj} / (\boldsymbol{\varepsilon}_{kj}\, \mathbf{G}_{kj}\, \Delta E_{kj}) \quad (11)$$

Therefore, the first goal of calibration is to obtain detector-channel-averaged transfer factors $\mathbf{H}_{kj}$ (or the equivalent efficiency factor $\boldsymbol{\varepsilon}_{kj}$ since $\mathbf{G}_{kj}$ is easy to calculate), the detector-channel energies E_{kj} and the detector-channel energy band pass ΔE_{kj}.

More quantitative work may require a full inversion of the kernel equation given in Equation (9). Here we are usually aided by the fact that to some level of approximation the Transfer Function **T** is separable in the form:

$$\mathbf{T}(S, E, \theta, \phi) = \mathbf{K}(S, E) * \mathbf{P}(\theta, \phi) \quad (12a)$$

and hopefully even

$$\mathbf{T}(S, E, \theta, \phi) = \mathbf{K}(S,E) * \mathbf{C}(\theta) * \mathbf{D}(\phi) \quad (12B)$$

Note that even with these separations, an exact inversion of the integral is rarely possible, and we can compute only the coefficients of some tailored expansion of **K**, **C**, and **D**, as for example in spherical harmonics (using Legendre polynomials). The accuracy of these coefficients depends on both the raster coverage of the measurements and on the calibration.

Goals of the EPS characterization and calibration efforts

The goal of EPS characterization and calibration efforts, then, is to relate the rates, $\mathbf{R}_{kj}$, of the on-board or ground-defined channels to the in situ particle intensities $\mathbf{I}(S, E, \theta, \phi)$ by developing a hierarchy of information about the EPS Transfer function $\mathbf{T}(S, E, \theta, \phi)$. Specifically, we wish to derive for each channel:

$$E_{kj},\ \Delta E_{kj},\ \boldsymbol{\varepsilon}_{kj}\ \mathbf{G}_{kj\ j},\ \mathbf{C}_{kj}(\theta),\ \mathbf{D}_{kj}(\phi),\ \mathbf{K}_{kj}(S, E),\ \mathbf{P}_{kj}(\theta, \phi),\ \text{and finally,}\ \mathbf{T}_{kj}(S, E, \theta, \phi)$$

Clearly, the further to the right we move into this list, the higher the fidelity the characterization and calibration efforts must be.

Typical calibration procedure consists of stimulating the instrument with energetic particles, first from radiation sources, and then from accelerator beams (fair approximation of a delta function) and recording the response of the different channels. For EPS we must scan following variables:

- Species and Mass: e, H, He, O, Ar (proxy for heavier species, e.g. Fe)
- Energy: 1keV – 5MeV (~40 energies for 10 points/decade)
- Polar angle: +/- 10 deg (12 degrees nominal FOV)
- Azimuthal angle: +/- 90 deg (160 degrees nominal FOV

Note that even given this level of discreetness, complete characterization to the level of establishing $T_{kj}(S, E, \theta, \phi)$ for all channels requires: 5 masses * 40 energies * 21 polar angles * 180 azimuthal angles = 756,000 calibration points! Clearly it is not possible to run this many beam values without significant infrastructure and automation. Therefore, we are dependent to a substantial degree on the separability of the Transfer Function as described in Equation (12). An important goal of the characterization and calibration efforts is, in fact, to establish that degree of separability. Simulations play an important role in establishing expectations for the instrument, as discussed in the next section.

4.0 EXPECTED EPS PERFORMANCE AND SIMULATIONS

Described here are the calculated expectations regarding the performance of the EPS instrument. We describe various calculations and simulation runs that provide a higher level of fidelity in predicting the performance of the EPS instrument than those based on experience with previous instruments. These simulations constitute the benchmarks against which subsequent ground and flight calibrations are to be compared. A table of expected EPS performance characteristics is provided at the end of this section (Table 4.1)

Numerical simulation provides an efficient and effective mean of verifying and quantifying the flight instrument response. Hence, a range of simulation tools are developed in order to characterize EPS. The results from these simulation tools allow us to calculate the end-to-end expected performance of the instrument which one can use to compare with in-flight and calibration data. Different sections of EPS are simulated using different tools to gain better understanding on each part of the instrument. Three major sections are simulated separately: 1) Collimator; 2) TOF section, and 3) Solid State Detector (SSD).

Collimator Performance and Geometric Factor

Collimator Geometric Factor. Figure 7 shows the collimator of EPS, as described in section 2. It consists of four concentric half circular plates that have holes aligned with a common point of origin at the center of the EPS TOF telescope. The size and number of collimator holes define the geometric factor **G** of the instrument. The many-holes collimator design minimizes the scattering of ions and electrons at the collimator while restricting the field-of-view (FOV) of the instrument. The geometric factor of a single set of aligned holes, with outer-hole and inner-hole diameters of 2.34 and 1.68 mm, with holes separated by 1.3 cm, is 0.00056 cm^2 sr. With 33 x 4 holes, the geometric factor G for the entire collimator is 0.074 cm^2 sr. Assuming that each species on each SSD is allotted $1/12^{th}$ of that amount, the $\mathbf{G}_{kj}$ value is roughly 0.0062 cm^2 sr. $\mathbf{G}_{kj}$ for the Low Energy Ions (TOF-only) is roughly twice that value, or ~0.012 cm^2 sr. Note that the needed Transfer Factor $\mathbf{H}_{kj}$ depends also on the counting efficiency $\boldsymbol{\varepsilon}_{kj}$ which depends, in turn, on species and instrument mode.

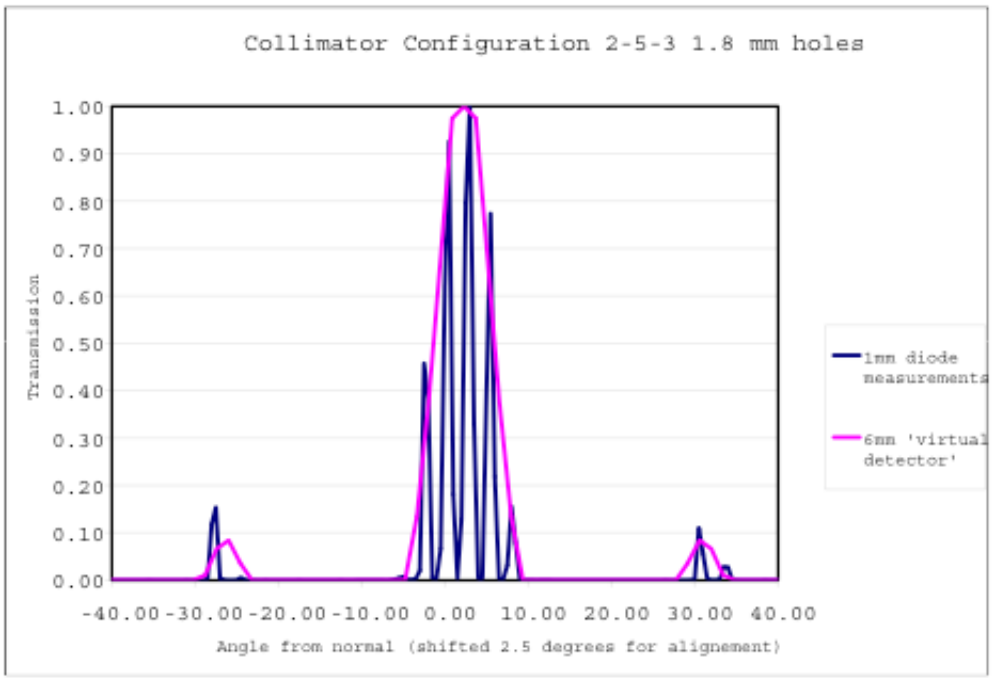

Figure 11. Simulation and laser light measurement of the EPS collimator performance

Collimator Side Lobes. This geometric factor calculation given above does not take into account the situation of particles coming through different set of holes (i.e. side lobes) that are not incorporated a detector with flight-like dimensions. An example of such side lobes is shown in Figure 11. Here, a Monte Carlo simulation and an independent laboratory measurement of a collimator were performed. The laboratory measurement (blue line; performed with laser light and a 1 mm wide photo diode) is compared with the simulation (shown in pink), which incorporated a detector with flight-like

dimensions. The real and the simulated detections were performed at the position where the SSD detectors are mounted. Both curves have been normalized to transmission of 100% at 0° incidence. The simulation results are in excellent agreement with the actual measurement with the collimator. The collimator used for this comparison is a prototype with slightly different characteristics from that used for flight. The prototype validated the simulation model, which in turn was used to refine the flight model characteristics.

A two-dimensional view of a simulation of the true flight-collimator transmittance characteristics is shown in Figure 12. Here the view is as it would be to a tiny bug sitting on the surface of one of the SSDs. The main side lobe resides about ±28.3 degrees on either side of the principal peak along the "alpha" direction along the main axis of the sensor (The principal peak is shown with saturated color values and positioned at [0, 0]). Each side lobes represent ~4 % of the transmitted flux, and the full width at half maximum (FWHM) of the principal peak is ~7.5°. Because Figure 12 is the response for a single position on a SSD, the instrument-level $\mathbf{C}_{kj}(\theta)$, $\mathbf{D}_{kj}(\phi)$, and $\mathbf{P}_{kj}(\theta, \phi)$ functions are calculated by convolving the square SSD sensor area (as transformed to a an angle) with the function displayed in Figure 12.

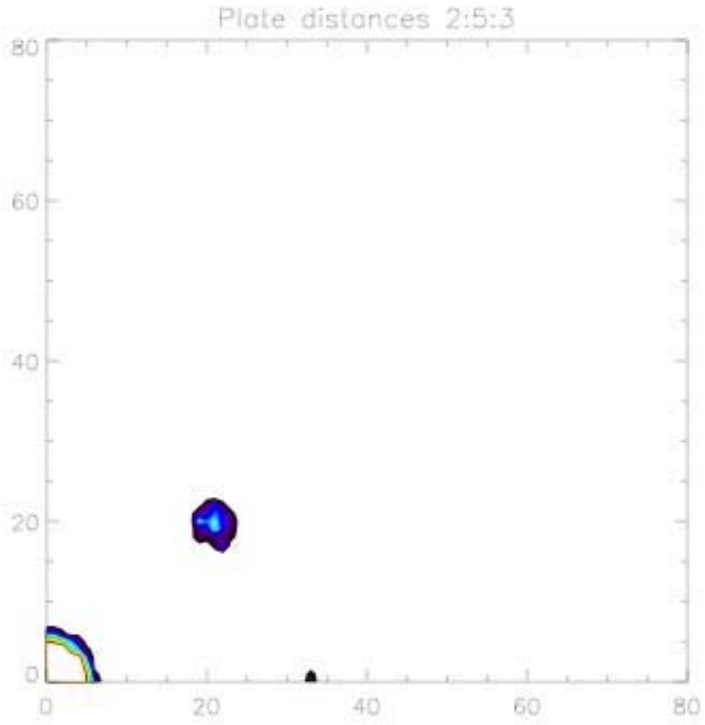

Figure 12. Monte Carlo simulation of the EPS collimator showing the side lobe as would be seen at a single spot on one of the SSD sensors.

Electron Scattering. Simulations using GEANT4 software (Agostinelli et al., 2003) were also performed to assess the collimator performance for suppressing electron scattering effects. Figure 13 shows the configuration used in the simulation along with some sample electron trajectories and secondary products (scattered electrons, x-rays). Simulations like this demonstrate that the electron counts detected in detectors adjacent to detector directly targeted by the collimator are just several percent of the counts observed in the targeted detector. The engineering prototype of EPS will be tested with electrons after the planned upgrade of the Johns Hopkins APL particle accelerator facility before about 2007.

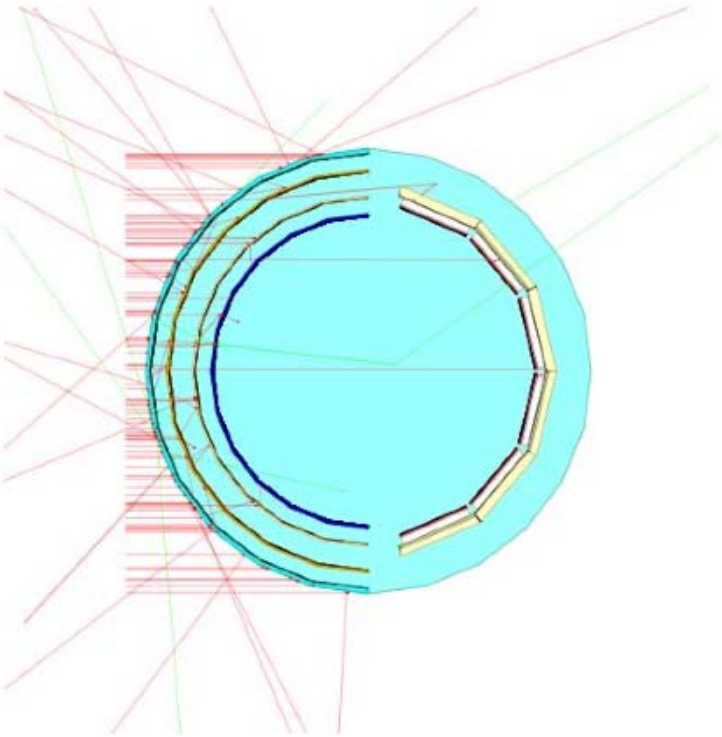

Figure 13. Top view of GEANT-4 sample simulation of EPS collimator plates. Energetic electrons are incident on EPS from the left into the instrument. Scattering inside the instrument has properly simulated. Red lines are primary and scattered electrons. Green lines are secondary x-rays.

Ion Measurements

Electron Optics. As discussed in section 2, secondary electrons generated by primary ions in a start and a stop foil are used to generate timing signals to measure the ion's time-of-flight (TOF) within EPS. They are also used to determine the directionality of the low energy ions that do not stimulate the SSDs.

Figure 14 shows sample simulated secondary trajectories within EPS from the foil to MCP, derived using the commercial COULOMB software (see web site: "www.integratedsoft.com/products/coulomb/"). Here, a pie-shaped cutout of the cylindrical EPS sensor is shown (cylindrical symmetry is assumed for the electrostatic fields). The electron optics for both the start foil/MCP and stop foil/MCP are identical, hence Figure 14 shows a good representation for both start and stop electron trajectories. Electrons are generated at the foil (right of the figure) when ions (not shown) transverse through the foil. These low energy electrons (typically <10 eV) are immediately affected by the accelerating voltages within EPS (the high energy ions are not significantly affected by the accelerating voltages) and are steered towards the Microchannel Plate (MCP; the flat surface on the top end in the figure) as evident in the figure. An important issue is the dispersion in the arrival times of the secondary electrons as a function of foil position and the angle of emittance of the secondary electrons from the foil. Such dispersion adds to the error in the measurement of time-of-flight. Figure 15a shows the time dispersion associated with varying angles for electrons emitted from the center of the foil. In Figure 15b the dispersion shown for any one column are associated with varying the emission position over the ~6 mm vertical extent of the foil. The combination of position and angle yields a time dispersion of roughly 1.5 – 2 ns. Combining the dispersions associated with the start and stop detections in a root-mean-square sense yields a total time dispersion error of roughly 2.1 – 2.8 ns. Combining that value in a root-mean-square sense with the ~1.5 ns electronic dispersion yields a total time dispersion that resides between 2.5 and 3.2 ns.

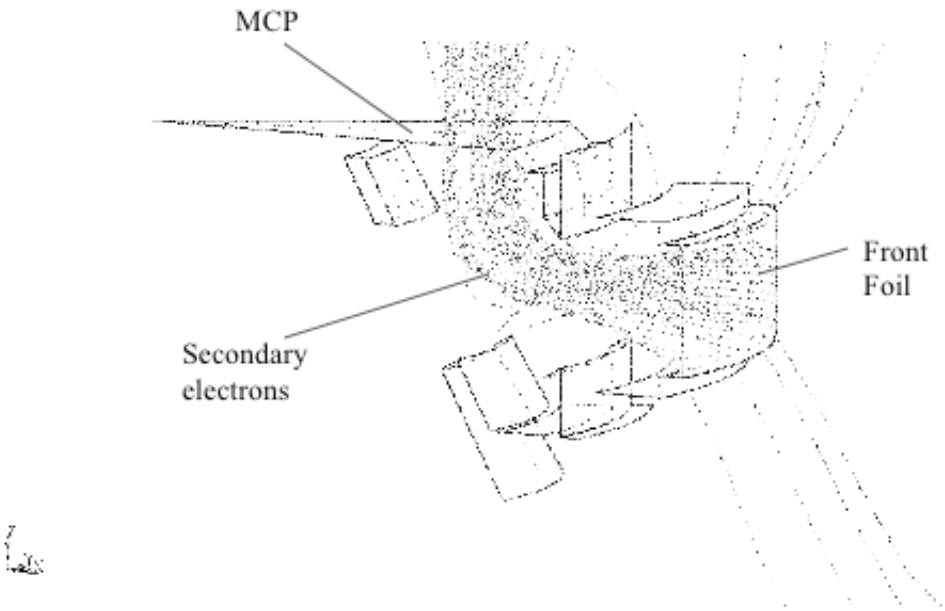

Figure 14. Simulation of secondary electron trajectories within part of the EPS TOF section.

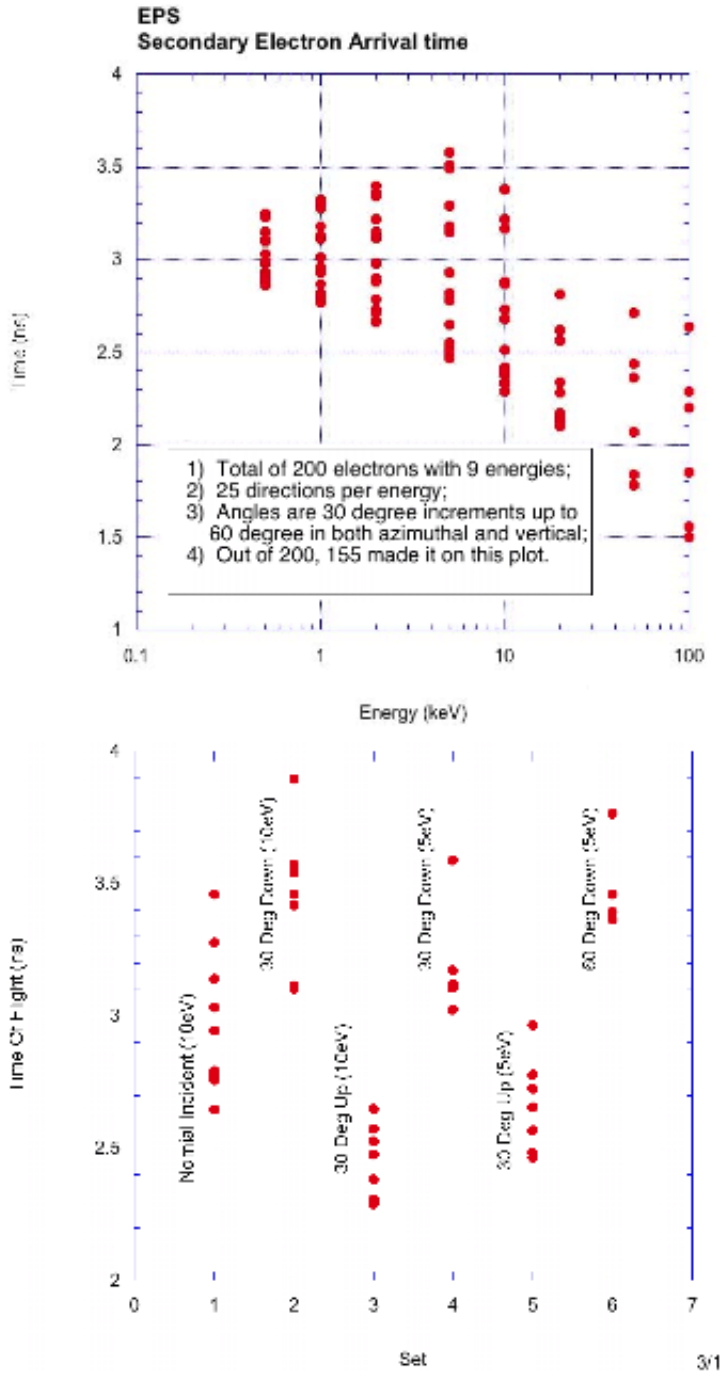

Figure 15. Simulation of the contribution of secondary electron transport to the time-of-flight dispersion.

Ion energy losses. As ions transverse the TOF section of EPS through the front foil (~10 μg/cm^2), back foil (~19 μg/cm^2), dead layer of the solid state detector (~550 Å), and eventually stop and deposit their total energy in the SSD, they will lose energy and scatter depending upon the ion's initial energy, mass and the medium through which they pass. We have incorporated data from the SRIM (Stopping and

Range of Ions in Matter; Biersack and Haggmark, 1980) particle-interaction-with-matter code in our simulation to simulate realistically the energy loss and scattering as ions transverse through different materials in EPS.

TOF measurements. When ions penetrate through the front foil, a distribution of ion velocities is created, as calculated using SRIM. This distribution of ions is then used to calculate the distributions of ion TOFs. The uncertainty due to secondary electron dispersion and electron noise together with SRIM data are all incorporated in our simulation. Figure 16 shows the simulated response of EPS TOF spectra as a function of particle initial energy for four species (H, ^{3}He, ^{16}O, and ^{56}Fe). At low energy (~10s of keV), ions lose significant amounts of energy and scatter significantly when going through the front foil. These effects explain the spread in TOF measurement at low energy. However, at higher energy (~100s of keV), the TOF spreads are mostly consequences of the uncertainties in the TOF measurement from both the electronics jitteri (~1.5ns), and secondary-electron dispersion in the TOF optics as discussed in previous section (except for very heavy ions, e.g., Fe).

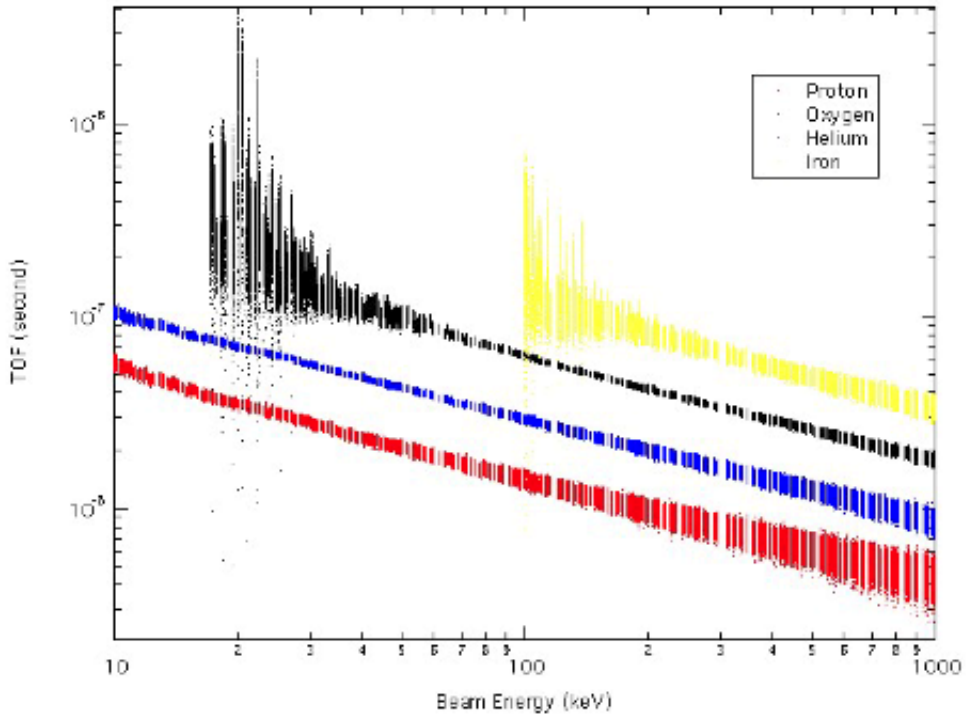

Figure 16. Simulated EPS TOF spectra as a function of accelerator beam energy for proton, oxygen, helium and iron. Red, blue, black, and yellow represent protons, helium ions, oxygen ions, and iron ions.

Total energy measurement. If an ion has sufficient energy left once it transits the front and back foil, it ends up in the SSD. Depending on the ion's final energy and mass when it reaches the SSD, it can penetrate through the dead layer of the SSD and produce an electronic signal to be measured. Figure 17

shows the simulated measured energy by EPS as a function of the ion's initial energy before entry into EPS. The measured energy shows the cumulative effect of the energy spread due to energy lost throughout the EPS (start foil, stop foil, dead layer, and electron hole pair production). The energy loss is greatest for ions with the greatest nuclear charge, here Fe.

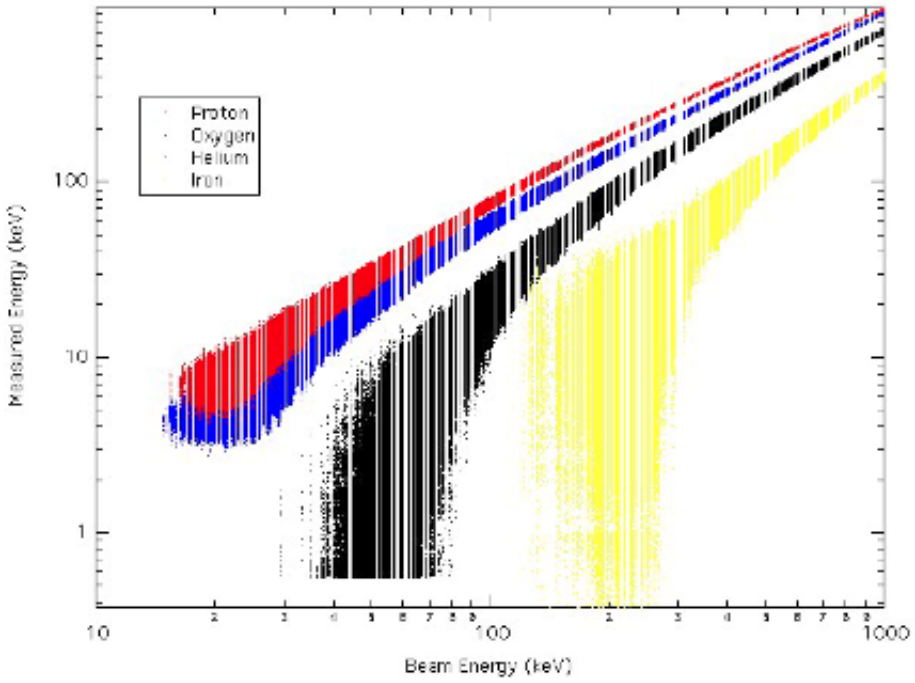

Figure 17. Simulated EPS measured energy versus incident energy for four different ions. Red, blue, black, and yellow represent protons, helium ions, oxygen ions, and iron ions.

TOF versus Energy. Finally, Figure 18 shows the result of combining the energy measurement with the TOF measurement on a particle-by-particle basis. Notice that even with a ~3 ns time dispersion, the major elemental species of interest (H, He, CNO, Fe) are discriminated except at the lowest energies for CNO and Fe, where the error in the energy measurements dominates.

Efficiencies. The efficiency for detection of an ion within the SSD's is roughly ~100% (except at the very lowest energies where energy straggling can position the energy below the low energy threshold). The efficiency for obtaining a TOF measurement is estimated using the efficiency of generating secondary electrons in both the front and the rear foil. To emit a secondary electron, such electrons must be generated close enough (distance "ρ") to the surface of the foil so that the electron can escape before it is re-assimilated. Thus, very roughly, it is expected that the efficiency for the generation of a secondary electron is proportional to the amount of energy per unit distance (dE/dX [keV/micron]) that an ion deposits as it goes through this outer thin layer of the foil. The canonical number of secondary electrons generated out of each surface as a proton with 10's of keV energy encounters the foil is between 0.5 and 1 (Frischkorn et al., 1983; D. W. McEntire, Private communication, 2004; estimated here as 0.75). Since we require a simultaneous start and stop electron, the efficiency of proton detection

at 10's of keV is $(1\text{-Exp}[-0.75])^2$, where 1-Exp[-0.75] is the Poisson probability of having at least 1 or more electrons emitted when the mean emission number is 0.75. Thus, the efficiency is roughly 22%. Other energies and species may be roughly scaled with this number using tabulated dE/dX values. For example, at 50 keV total energy the dE/dX values for protons and oxygen ions are 120 and 250 keV/micron, respectively (we ignore for now the energy losses suffered by the ion in getting to the position in either foil where the secondary electron is generated). Thus, since the average number of secondary electrons for oxygen will by ~0.75 x (250/120), or 1.56, Poisson statistics tells us that the probability of detecting an oxygen ion with 50 keV energy is $(1\text{-Exp}[-1.56])^2$ or 62%. Tables in Appendix 8 will provide calculations of expected efficiencies for the end energies (each end of the energy bandpass) calculated on the basis of a dE/dX scaling. In those tables, energy losses at intermediate positions within the instrument (i. e. at each of the two foils) are folded into the calculations. Not folded into those calculations are the differences between forward and backward secondary electron generation nor is the probability of the primary ion being scattered within the start foil to the extent that it misses the stop foil and the SSD array. The efficiency calculations in the Tables in Appendix 8 will be complete by 3/1/05, several months prior to the EPPS in-flight checkout period.

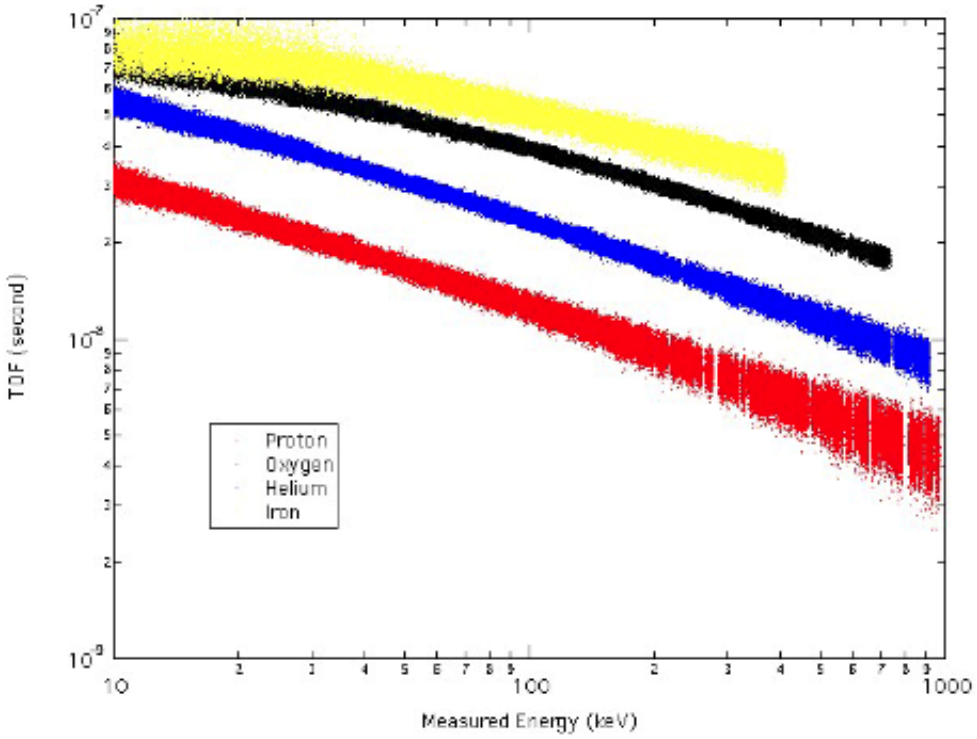

Figure 18. Simulated EPS TOF versus measured energy. Red, blue, black, and yellow represent protons, helium ions, oxygen ions, and iron ions.

Electron Measurements

The EPS electron measurement strategy depends on the use of the aluminum flashing on the electron SSD. We therefore need to understand the effect of that flashing on both the ion and electron measurements within the electron SSDs. Based on simulations with GEANT-4, Figure 19 shows the effect of Al flashing on proton measurements, and Figure 20 shows the effect on electron measurements, for a varying thickness of Al flashing. The baseline spectrum assumed for both protons and electrons is a power-law spectrum with a spectral index of 3; that is, Intensity = A E^{-3}, where "A" is a constant. With the flashing thickness utilized with EPS, 1 micron Al, the proton intensities are severely depleted for energies < 250 keV. With that flashing thickness, the electron intensities are maintained to energies down to about 20 keV. The dropoff of electron intensities at the highest energies occurs because of the electron penetration of the 500 micron detectors. That drop-off is rounded because of electron scattering within the SSD, as demonstrated with an examination of the detailed trajectories of individual electrons with the GEANT-4 simulations. There may be periods of time when the ion counts overwhelm the electron measurements. The most important issue is not that the electrons may be occasionally contaminated, but whether or not the electrons are contaminated in a way that we are fooled into thinking the ion counts are really electron counts. This problem is intrinsic to the technique used here to measure the electrons. Extensive experience with similar measurement made by the EPIC instrument on Geotail demonstrates that, because of the clean proton measurements (below and above 250 keV) made in roughly the same direction, it is unlikely that we will be fooled into thinking that ions counts are actually electron counts.

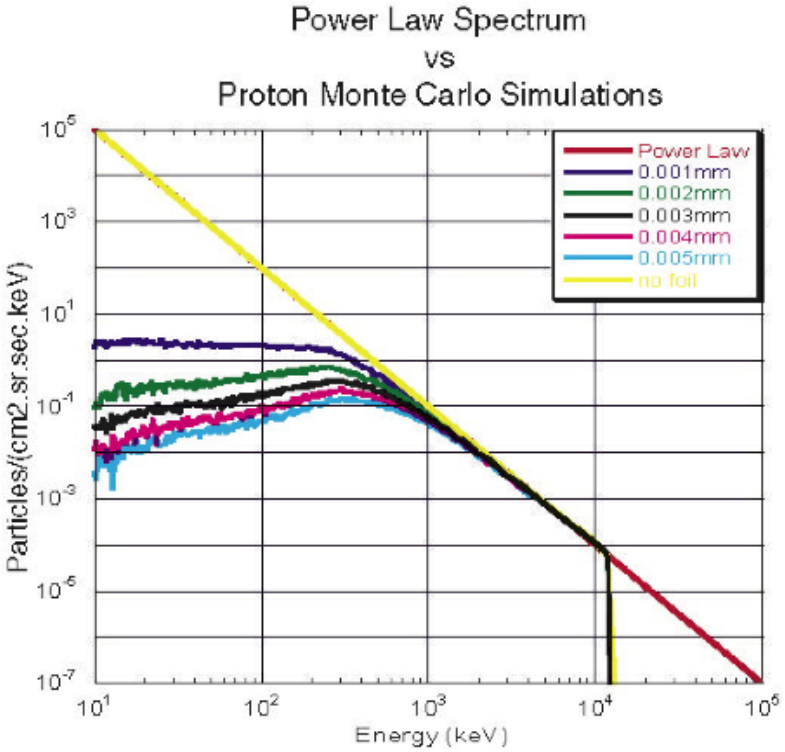

Figure 19. Simulated measured proton spectra for different Al flashing thickness from a known incident spectra on a 500 µm thick silicon detector.

In Figure 20 the "1-micron" flashing spectrum lies below the nominal input spectrum primarily because of scattering of electrons as they traverse the flashing and the SSD itself. The table of electron channels in Appendix 8 will show the nominal consequences of such scatterings on the mean energies and efficiencies associated with each channel, as will be calculated with GEANT-4.

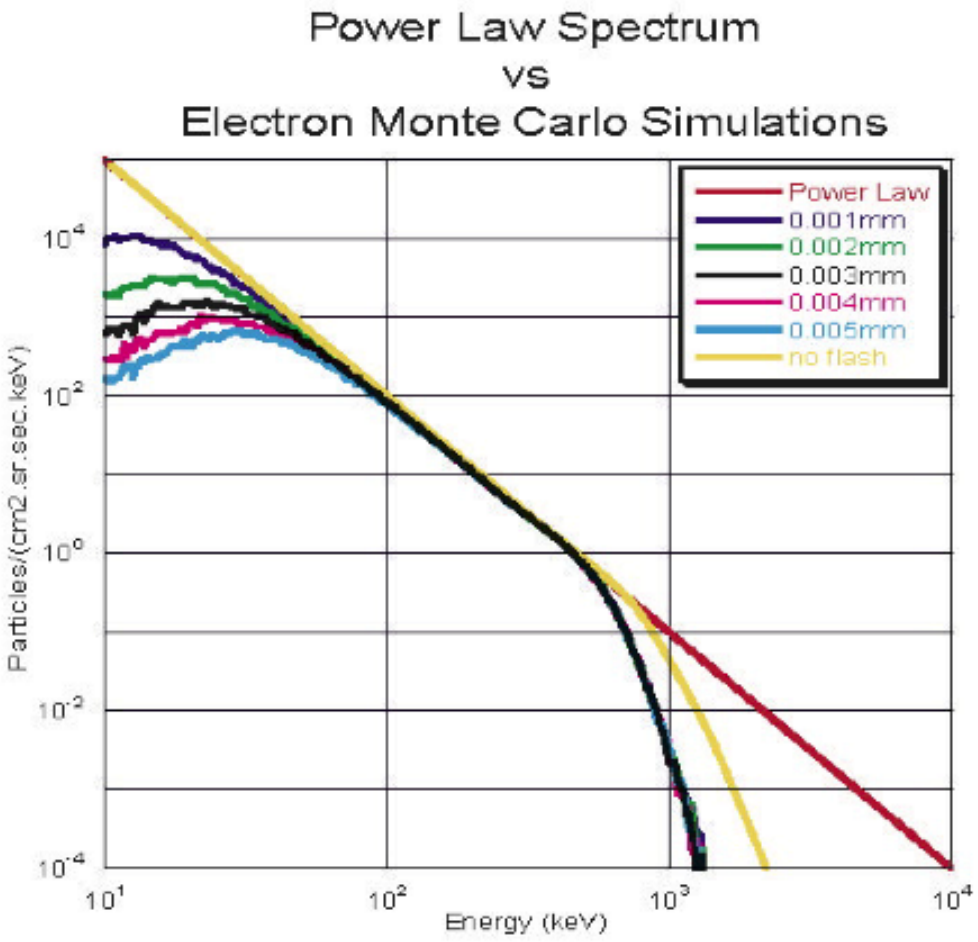

Figure 20. Simulated measured electron spectra for different Al flashing thickness from a known incident spectra on a 500 μm thick silicon detector.

Electron scattering off collimators and other sensor surfaces is always an issue with the measurement of electrons. The GEANT-4 simulations of the EPS instrument discussed in the section on the EPS collimator assure us that such scattering generates signals in non-illuminated SSD that are no more than several percent of the signal within illuminated SSDs.

Table 4.1 EPS Expected Performance

Geometric Factor (Instrument Total)		0.074 cm^2 sr
Geometric Factor (Electron Pixel)		0.0062 cm^2 sr
Geometric Factor (Low E Ion Pixel)		0.012 cm^2 sr
Geometric Factor (High Energy Ion Pixel)		0.0062 cm^2 sr
Geometric Factor (Diagnostic Ions)		0.0062
Electron Efficiency vs. Energy		Roughly 100%. Details in Appendix 8 (TBS 3/1/05)
Low Energy Ion Efficiency vs. En x M		> 20% anticipated. Details in Appendix 8 (TBS 3/1/05)
High Energy Ion Efficiency vs En x M		>20% anticipated Details in Appendix 8 (TBS 3/1/05)
Diagnostic Ion Efficiencies		~100%
Energy Coverage		See Table Below
ΔE / E capability at 50 keV		16%
ΔE / E capability at > 100 keV		< 8 %
Energy / TOF Channel resolution		Electronic channels in Appendix 8. Primary particle characteristics TBS 3/1/05
TOF dispersive spread		2.5 to 3.2 ns
Mass Species Separation		See Table Below
Angular Coverage (total)		160° x 12°
Angular Coverage (Electrons)		147° x 12°
Angular Coverage (Low Energy Ions)		160° x 12°
Angular Coverage (High Energy Ions)		147° x 12°
Angular Coverage (Diagnostic Ions)		147° x 12°
Angular Pixels (Electrons)		12° x 27° (13° with 13.6° gap)
Angular Pixels (Low Energy Ions)		12° x 27° (full ~27° coverage)
Angular Pixels (High Energy Ions)		12° x 27° (13° with 13.6° gap)
Angular Pixels (Diagnostic Ions)		12° x 27° (13° with 13.6° gap)
Electron Scattering Angle Contrast		Several percent
Collimator Side-Lobes: Position		(Δα, Δβ) = (±28.3°, ±0°)
Collimator Side-Lobe Fraction/Lobe		~4% per lobe
Energy Coverage:		**Technique**
Electrons	15 keV – 0.6 MeV	Singles / Foil Technique
LE Protons	5 keV – 1 MeV	TOF + PH Discrimination
LE CNO	15 keV – 3 MeV	TOF + PH Discrimination
HE Protons	15 keV – 2.8 MeV	TOF vs. Energy
HE He	25 keV – 2.8 MeV	TOF vs. Energy
HE CNO	60 keV – 3 MeV	TOF vs. Energy
Diagnostic Protons	15 keV – 2.8 MeV	Singles
Energy / TOF Channels		Electronic channel definitions. In Appendix 8. Primary particle characteristics TBS 3/1/05.

Summary of Anticipated EPS Performance.

Table 4.1 summarizes the expected performances of the EPS instrument based on the calculations and simulations described in this chapter.

5.0 FLIGHT EPS CALIBRATION

Here we document the calibration of the flight instrument that is now (29 May 2004) mounted onto the spacecraft. These calibrations primarily established the basic functionality of the instrument, but left open a number of questions that are being addressed with a flight-like engineering model (Sections 6). Final calibration will be established in flight with a plan that takes advantage of much that we have learned, and will learn, with the engineering model (Section 7). The calibrations were performed using a degraded (energy spread) Am-241 alpha-radiation source and an ion beam accelerator facility recently established at JHU/APL. The JHU/APL calibration facilities are described in Appendix 9. At present, the calibration sources and the test facilities generate only ions. The functionality of the electron sensors in EPS have, to date been established with protons with sufficient energy to penetrate the Al flashing on the electron sensors. From the detector functionality perspective, protons serve just as well as electrons to stimulate the electron SSDs and demonstrate that the electron signal processing chains operate well for the range of SSD energy depositions needed to characterize the ~25 to 500 keV electron energies of interest. The question that remains following such proton calibrations of the electron channels is whether the scattering property of the electrons gets in the way of establishing the directionality of the electrons. Our full-up, detailed geometric simulations of the electron performance of EPS using GEANT4 show that scattering randomizes the directionality of less than several percent of the electrons.

Tests Set Up

For the accelerator beam tests, the output of the accelerator described in Appendix 9 was attached to a ~1 m diameter and ~1 m tall cylindrical vacuum chamber evacuated to $< 10^{-6}$ torr. The EPS instrument was mounted to a rotating turn-table that allowed the allowed the beam to be scanned over 5/6 of the ~160° alpha dimension. (Rotation was possible only in one dimension.) The response of the instrument to beta-angle variations (i. e. over the ~12° FOV dimension) was not investigated with the accelerator beam. Also, during the tests where the turn-table was free to rotate, the instrument tended to overheat because of poor thermal coupling with the surrounding structures. Therefore the angular response of the instrument was investigated only for basic functionality. For most of the tests reported here, the angular position was frozen so that a liquid-nitrogen cooling system could be attached to the EPS sensor.

Directionality

Calibration runs like those depicted in Figure 21 document the ability of the EPS sensor determine the directionality of the incoming charged particles. Figure 21a shows the ability of the discrete "start" anodes to determine the directionality of the incoming particles for the Low Energy Ion events (no SSD signals). For this particular test, the collimator on this flight unit was not installed (Some tests are run without the collimator because the small hole pattern of the collimator interferes with the pencil-like characteristic of the accelerator beam in a fashion that makes it difficult to quantify the response of the

detector.) The beam was confined to shining on one small portion of the start foil by the narrowness of the ion beam. Figure 21b shows the ability of the discrete SSD's to determine the directionality of those high-energy ions that stimulate the ion SSD's.

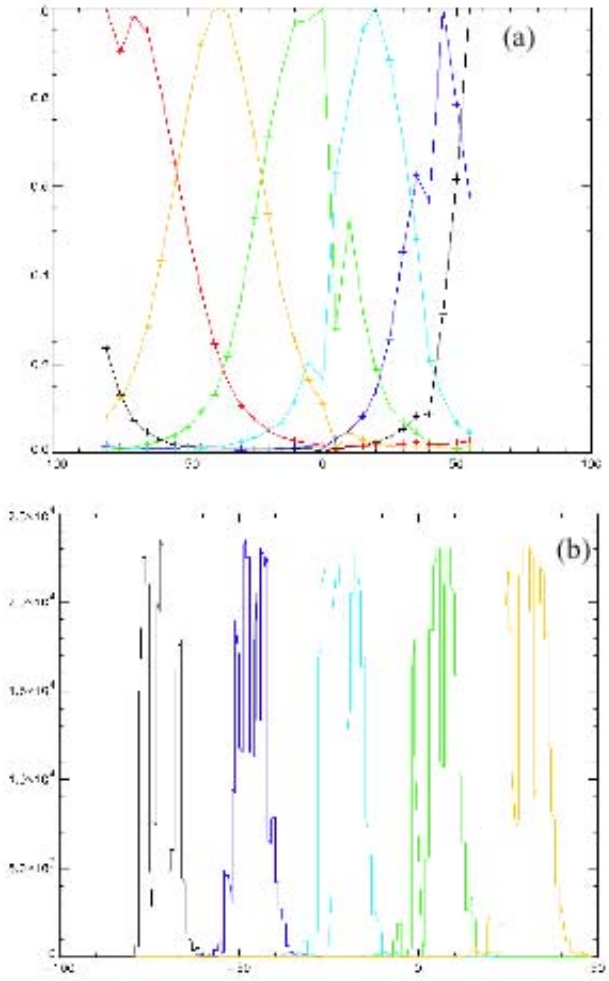

Figure 21. (a) Angular scan in the "alpha" direction of uncollimated EPS showing response of discrete start anodes to narrowly collimated proton beam (140 keV). The discrete anodes perform the imaging function for Low Energy Ions. The best FWHM resolution achieved here (light blue curve is ~30 degrees as compared to ideal ~27 degrees. (b) Angular scan in the "alpha" direction of collimated EPS showing response of the ion SSD pixels to a narrowly collimated proton beam (140 keV). The observed FWHM resolution achieved (~13 degrees with ~13 degree gaps) is in agreement with expectations. The proton beams used have angular spreads on the order of ~1 degree. The angular resolution achieved is adequate for the science to be performed. There are no explicit (CSR) requirements on angular resolution.

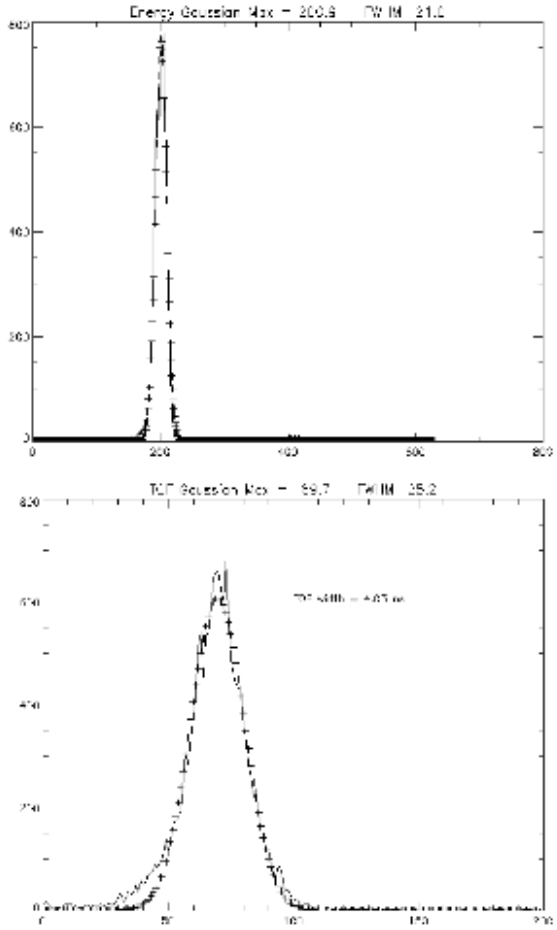

Figure 22. The gaussian fits of the energy and TOF and the observation histograms for Run #7 is shown is this figure. The input beam was a 170 keV mono-energetic protons. The Gaussian Maximum of the energy was in bin 200.9 and using the function E = bin*0.57387 (keV) indicates a energy deposition of ~115 keV with a width of ~12 keV. Significant energy loss through the foils was observed in this run as the beam started out at 170 keV. The TOF peak was in bin 69.7 and using the function TOF=bin*0.16276 (ns) indicates the TOF for these protons was ~11.3 ns with a ~4 ns FWHM.

Issues that need to be addressed includes the level of electronic cross-talk between the adjacent discrete start anodes and the level of cross-talk between the different pixels of each SSD wafer (each SSD wafer has 4 pixels). The cross-talk between start anodes will comprise some combination of electronic noise and cross-anode drift of secondary electron trajectories. These two effects will be sorted out with the engineering model and our simulation model of secondary electron trajectories (Section 4). Cross-talk between SSD pixels will be quantified with the engineering model. The engineering model is constructed to be sufficiently flight-like to reproduce the flight model characteristics.

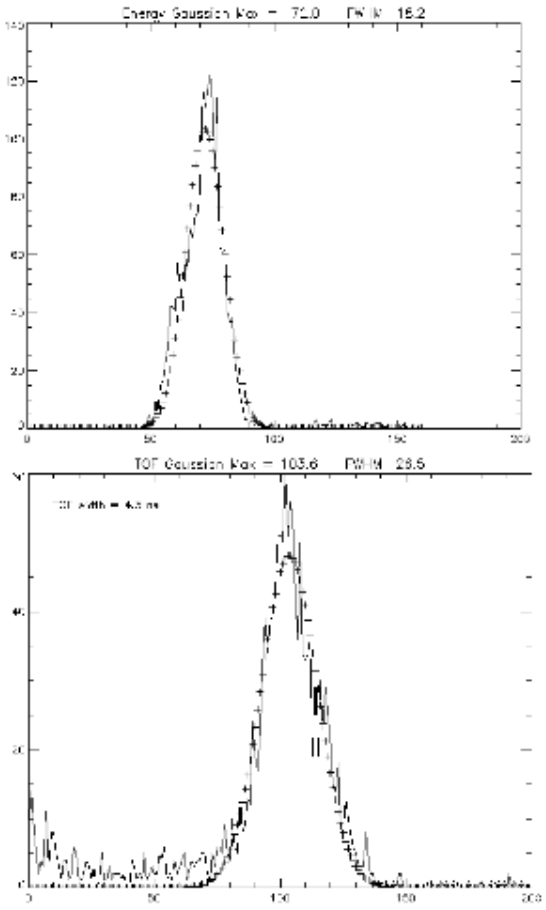

Figure 23. The gaussian fits of the energy and TOF and the observation histograms for Run #1 is shown is this figure. The input beam was a 80 keV proton beam and as the histograms indicate was broader than at higher energies. The Gaussian Maximum of the energy was in bin 72 and indicates a energy deposition of ~41 keV with a width of ~10 keV. The TOF peak was in bin 103.6 and indicates the TOF for these protons was ~17 ns with a ~4 ns FWHM. The events outside of the main peak are accidentals (due to other emissions from the calibration beam) and are discriminated against with the triple coincidence requirement in the final data stream.

Calibration Beam Runs

Throughout most of the calibration activities where EPS was tested within the JHU/APL Calibration facilities, various problems were diagnosed (noise, FPGA programming, etc.) and were fixed. Following the finalization of the EPS configuration for delivery and following the introduction of cooling hardware within the calibration facility to keep the EPS head at a temperature of ~0° C, a series of calibration runs were performed that constitute our best knowledge of the performance of the EPS instrument at the time of delivery. Those calibration runs are listed and described in Appendix 10.

Unless otherwise indicated, the figures discussed here are taken from the calibration runs documented in Appendix 10.

Energy Resolution. Figures 21 through 25 show the energy and time-of-flight analysis performed for calibration runs #7, #1, #22, and #26, representing beams with 170 keV H^+, 80 keV H^+, 170 keV O^+, and 110 keV O^+. FWHM energy resolutions achieved are: 12, 10, 12, and 15 keV. These values are within a factor of 2 of expectations (Table 4.1) and are dominated by noise pickup from the power supplies, so it is thought. These results represent satisfactory performance and meet the requirements of the EPS system.

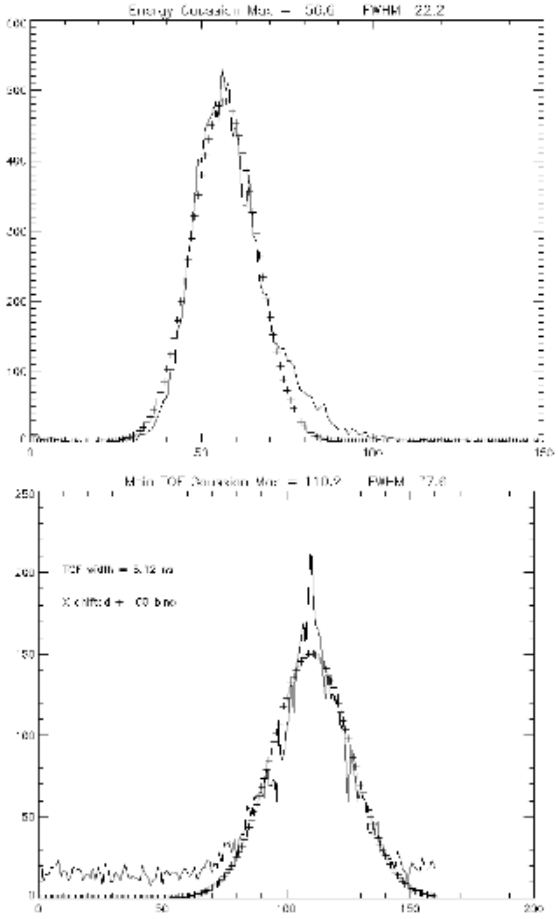

Figure 24. The gaussian fits of the energy and TOF and the observation histograms for Run #22 is shown is this figure. The input beam was a 170 keV oxygen beam. The Gaussian Maximum of the energy was in bin 56.6 and indicates a energy deposition of ~32 keV with a width of ~12 keV. Significant energy loss through the foils was observed in this oxygen run as the beam started out at 170 keV. The TOF peak was in bin 210.2 and indicates the TOF for these oxygen ions was ~34 ns with a ~6 ns FWHM. The events outside of the main peak are accidentals (due to other emissions from the calibration beam) and are discriminated against with the triple coincidence requirement in the final data stream.

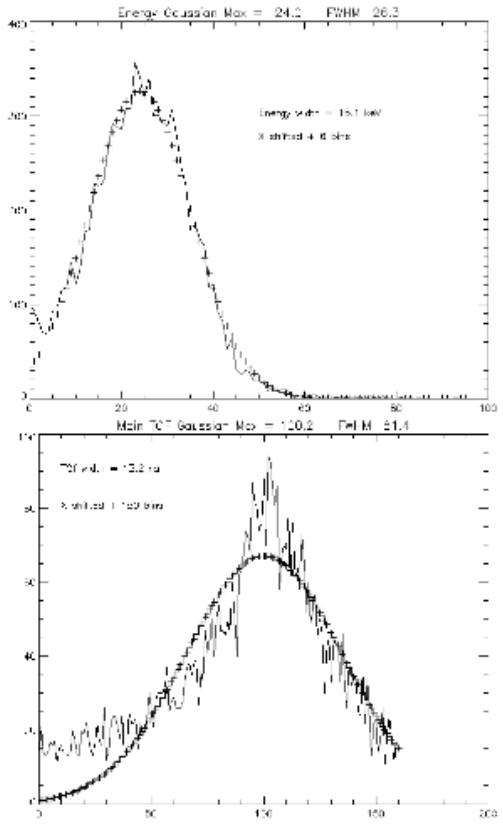

Figure 25. The gaussian fits of the energy and TOF and the observation histograms for Run #26 is shown is this figure. The input beam was a 110 keV oxygen beam. The Gaussian Maximum of the energy was in bin 30 indicates a energy deposition of ~17 keV with a width of ~15 keV. The TOF peak was in bin 250.2 and indicates the TOF for these oxygen ions was ~41 ns with a ~13 ns FWHM. The events outside of the main peak are accidentals (due to other emissions from the calibration beam) and are discriminated against with the triple coincidence requirement in the final data stream. Here imperfect operation of the accelerator (we are on a learning curve) have cause spurious events to contaminate the response peak. The full width at half maximum still provides a rough estimate of the resolution capabilities.

Time-of-flight Resolution. The FWHM of times-of-flight for the 4 examples shown in Figures 21 through 25 are ~4, ~4, ~6, and ~13 ns. We have found that, intrinsically, the TOF spread ranges between ~4 and 6 ns for the EPS instrument as delivered to the spacecraft. When EPS was delivered to the spacecraft we did not understand why the TOF spread was substantially broader than anticipated (< 2 ns). We now understand that there are two causes: 1) the dispersive spread in the secondary electrons is broader than anticipated (~3 ns; Section 4), and 2) the performance of the Constant Fraction Discriminators (CFD) that analyze the timing pulses requires a higher bias voltage than previously appreciated in order that they follow the fast-changing MCP pulses. As documented below, the CFD bias is adjustable, and it is believe that a ~3ns TOF spread will be achieved by EPS in flight.

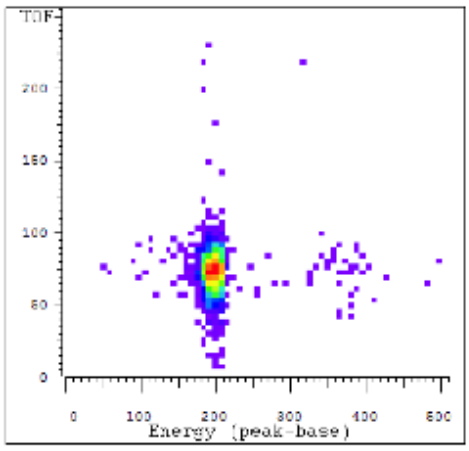

Figure 26. This 3D spectra is a screen capture of run #7, the 170 keV proton beam.

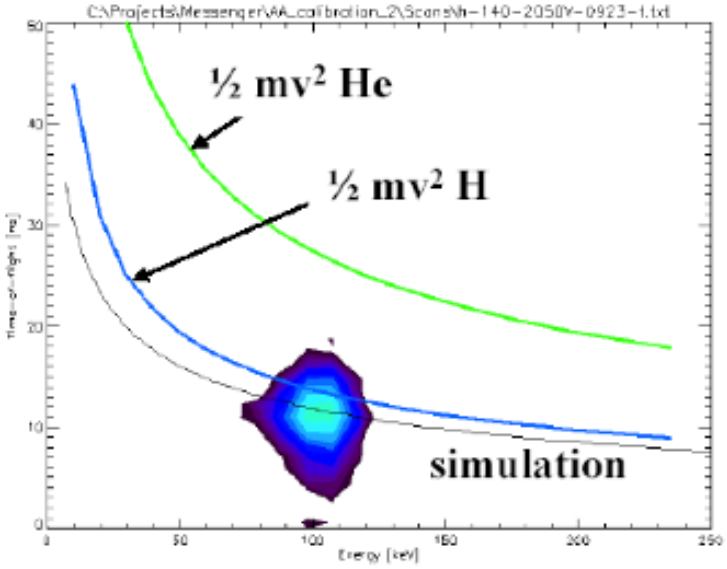

Figure 27. Time-of-flight versus energy display for a 140 keV proton beam with energy and TOF spreads of 16 keV and 4 ns, respectively (Run #5). With the overlaying theoretical expectations for protons and helium, the plot demonstrates the ability of EPS to discriminate different mass species despite the relatively broad energy and TOF spreads.

Time-of-Flight Versus Energy. Figures 26 through 30 illustrate the characteristics of simultaneous Energy and TOF measurements. Figure 26 shows a GSEOS screen capture of a 170 keV proton beam measurement, the same run used to obtain Figure 22. Figure 27 places a similar measurement (Run #5, 140 keV protons) in the context of the theoretical expectations for protons and helium ions. The figure demonstrates that, despite the somewhat broader energy and TOF spreads than those anticipated, relatively clean separation of the major mass species is anticipated. The bottom panel of Figure 28

shows the TOF versus Energy characteristics as revealed using an energy-degraded Am-241 alpha source. That same data is replotted (as individual points) on the top panel of Figure 28, and represented as green crosses. With the TOF spread of ~5 ns, clean mass discriminations between H and He above ~1 MeV total energy may be problematic. With the anticipated improvements, discrimination to several MeV should be possible.

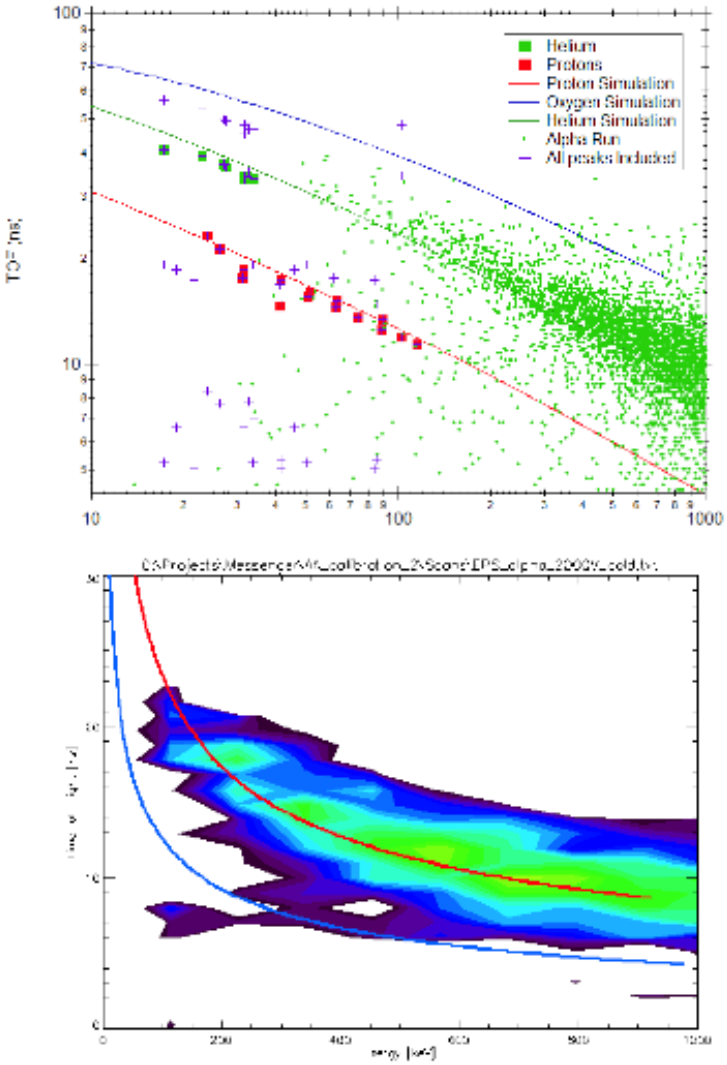

Figure 28. TOF vs Energy spectra. The points are data from several accelerator runs while the green dots are from an alpha source that was done with core code (i.e. not using the GSE software). The green dots are roughly on the alpha track simulated with the SRIM software while the other accelerator points lie close to their appropriate tracks as well.

The square red and green symbols represent the peak intensities of ion beams unambiguously identified as hydrogen and helium ions. These peaks fall relatively close to theoretical expectations. Figure 29 shows additional points. Our experience with the JHU/APL accelerator was, at the time of these calibrations, limited, and we did not always know the species and charge states of the various

components that came out of the JHU/APL ion accelerator. In some cases for the additional points plotted in Figure 29, charge states were assigned in a fashion that cannot be proven. . The figure suggests, but does not prove, that EPS identifies the different major mass species according to expectations.

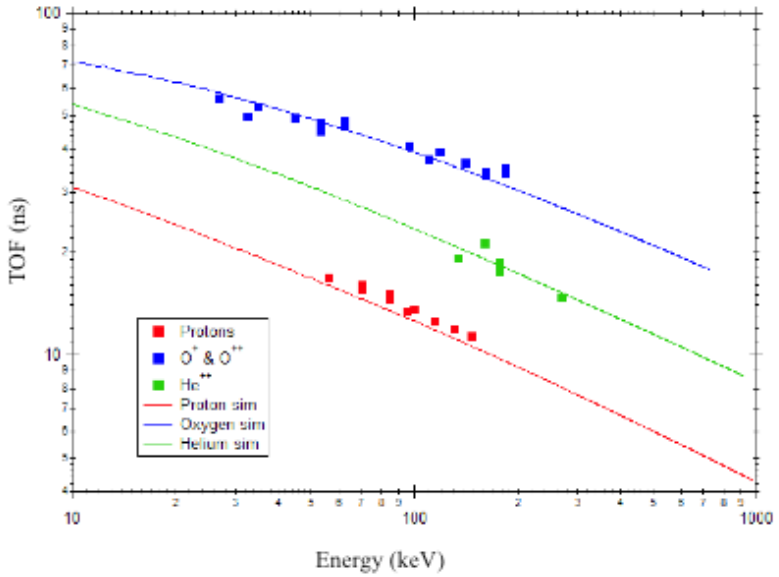

Figure 29. All data are accumulated from various accelerator runs. The red dots are where they should be (protons). Based on inexperience with the new JHU/APL accelerator, the charge state of heavy ions is not always known. If one assumes the various charge states indicated in the legend the dots fall on the appropriate simulated tracks.

Cross Talk? There is the suggestion in the calibration data that there exists some cross talk within the FPGA sorting of the different particle events. Some GSEOS screen captures like that shown in Figure 30 suggest that, when multiple species are present, some fraction of the TOF of one species may be paired with energy of another species. Extensive pulser tests have failed to identify this potential failure mode, and so, at this point in time, the issue remains open. Since the data like those shown in Figure 30 were accumulated, we have discovered that the Constant Fraction Discriminators (CFD) have been operated with non-optimal settings, and future tests with the engineering model will be performed to evaluate the presence - or absence - of such cross talk.

Efficiency. Efficiency of ion counting has been a continuing problem with the EPS instrument during the early phases of the calibration efforts. A rough estimate of ion TOF-only and TOF versus E counting is provided in the 27th and 28th rows of the Table in Appendix 10. These two estimates are obtained by dividing the "valid TOF" events and the "ion events", respectively, by the SSD Fast Counts. Note that for runs with multiple peaks, this estimate can easily be a factor of 2 in error. Once CFD discrimination levels were adjusted downward beginning with Run #9, reasonable TOF-only efficiencies were achieved. Note, for example, the efficiencies of 16.5% and ~23% during the proton Runs #15 and #23, respectively. We noted in Section 4 that efficiencies of order 22% were expected for protons.

However, the "ion event" efficiencies, depending on simultaneous TOF and energy measurements, reside in the neighborhood of a fraction of 1 percent.

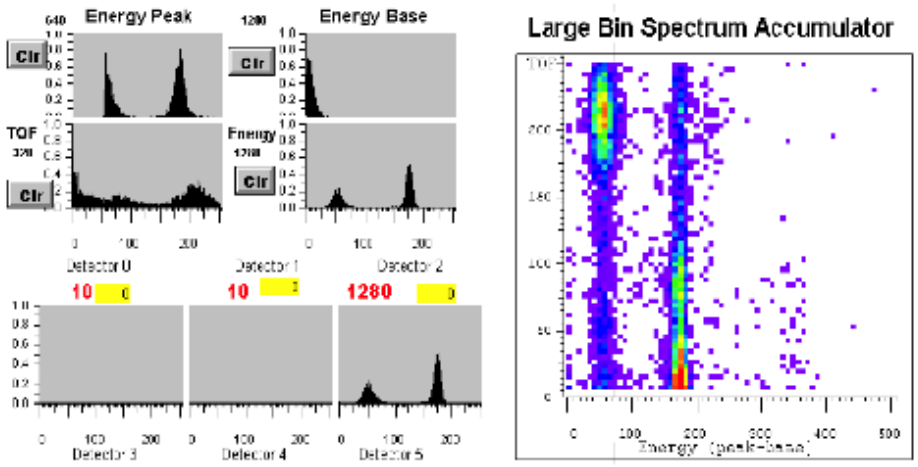

Figure 30. GSEOS screen capture illustrating an apparent cross-talk between the simultaneous identification of different mass species. There is the possibility that sometimes the energy of one species gets paired with the time-of-flight of another species. The problems with the Constant Fraction Discriminator settings was not yet identified at this time.

As described below, post-delivery testing of the EPS engineering model indicates that high-efficiency operation requires higher MCP voltages than were achieved during the pre-delivery testing to yield a higher gain out of the MCP. It appears that pre-delivery testing required multiple secondary electron emissions from the start and stop foils. Overall sensor efficiency is highly sensitive to this condition. A less than 10% probability of generating sufficient secondary electron signal on the start and stop anodes yields a < 1% efficiency for generating TOF-vs-electron events. Still puzzling is the relatively high efficiencies achieved with the TOF-only events. All of the results presented in this section regarding resolutions and mass separations are based on demonstrably valid TOF-versus-Energy events, not on TOF-only events.

Spacecraft Integration and Test Calibrations: TOF performance

Some understanding of the wider-than-expected TOF spreads was achieved with a combination of tests with the engineering model calibrations and flight-model during the spacecraft Integration and Test (I & T) activities. Post delivery engineering model testing revealed that the performance of the Constant Fraction Discriminators (CFD's) that process the start and stop signals from the MCP anodes are more sensitive to bias voltage than anticipated. At low biases the CFDs apparently do not work fast enough give the speed of the MCP pulses. During spacecraft I&T, an Am-241 radiation source was positioned so that it illuminated the entrance aperture of the flight EPS. Using bias settings for the CFD's

commensurate with those values used during the accelerator beam calibrations yielded TOF spreads of order 4 ns. When the bias voltage was increased substantially, TOF spreads of order 2 ns were achieved. We now understand with the engineering model tests that followed the I&T activities (as described in the next section), that the TOF spread is somewhat sensitive to the CFD discrimination values, and so we do not believe that < 2 ns TOF spread will be achieved once the instrument settings are fully optimized. However, we believe that we now understand the sources of the TOF spreads, and that the expected performance presented in Table 4.1 (somewhere between 2.5 and 3.2 ns) will be achieved. Thus, we anticipate achieving clean mass discriminations to the highest energies addressed with the EPS system, ~3 MeV.

Summary of EPS flight-model calibrations

Ion-beam calibrations of the flight EPS instrument demonstrate that energy resolution (FWHM) of between 10 and 15 keV is achieved, which, while being a factor of 1.5 to 2 larger than is achievable with SSD sensors and electronics of the sort used here, is nonetheless adequate for meeting the MESSENGER EPS requirements. For most of the calibration runs reported here, the observed TOF resolution (4-6 ns) was of the order of a factor of 2 wider than anticipated and could limit the ability of EPS to discriminate the major species H, He, and the CNO group at energies larger than ~1 MeV. However, during the I&T period calibrations of the EPS flight instrument, data acquired indicate that the anticipated TOF resolution of between 2.5 and 3.2 ns will be achieved in flight, so that clean separation of the major species (H, He, CNO group) will be achieved over the entire range of energies covered by EPS: >5keV/nucleaon to ~3 MeV total energy.

The major outstanding issues following calibration of the EPS flight model include: 1) low ion counting efficiencies, and 2) possible cross-talk in the identification of different mass species. Major progress has been made in addressing the first issue with the engineering model, as described in the next section. The second issue awaits attention. Given that the cross-talk flaw is not revealed with extensive testing of the species identification firmware using pulsers, it is, perhaps, a reasonable expectation that the cross-talk issue will disappear once all other sensor parameters, including MCP gain (next section) and CFD performance, are optimized.

6.0 ENGINEERING MODEL CALIBRATIONS

A flight-like engineering model of EPS has been developed and is now complete. Detailed calibrations of this model will begin in November of 2004 and will be completed by ~1 June 2005.. Some calibrations have already taken place with this unit at various stages of its construction. The differences between the flight EPS and the engineering model used for the test to date are that the engineering model has had only 2 SSD's installed, and it utilized so-called "rimmed" MCP's rather than the rimless MCP used for flight. The rimless plates are used for flight because they are considered more likely to survive handling and launch environments. Rimmed plates, on the other hand, are likely to outgas much more quickly than are the rimless plates, give the mounting configuration used with EPS. Two issues have been addressed to date: 1) the efficiency of ion counting, and 2) TOF spread performance.

Ion Counting Efficiency

For the engineering model of EPS, a critical issue has turned out to be the length of time that the unit has spent outgasing. For this test on ion counting efficiency, the MCP were allowed to outgas for several weeks within a high vacuum environment. After this outgasing, MCP plate voltages were raised to ~2300 volts, and the CFD thresholds were lowered to values (60 Hex) substantially below those achieved with the calibration runs documented in Appendix 10, all without the MCP start and stop rates reaching unreasonable values. Using an Am-241 alpha-particle radiation source, counting efficiencies of TOF-versus-energy events were as high as 35% (based on a ratio of triple coincident "ion events" and the SSD counting events). Further such testing will be performed beginning in Novermber of 2004 and will be complete by ~June 2005. However, the engineering model has demonstrated to date that the ion counting efficiencies commensurate with the theoretical expectations described in Section 4 are achievable with EPS.

TOF-Spread Performance

To investigate the factors that control the TOF spread, the engineering model was exercised by varying several of the EPS parameters, specifically the MCP plate voltage, the CFD discrimination values, and the CFD bias voltages. In this case the engineering model was configured with flight-like rimless MCP plates, and again, the unit was allowed to outgas for several week within a high vacuum environment. Sample results are shown in Table 6.1 below.

Table 6.1 Engineering Model TOF spread performance.

MCP voltage	**CFD Discrim.**	**CFD Bias**	**TOF FWHM**
(V)	(mV)	(V)	(ns)
1910	12	3.6	4.2
2030	12	3.6	2.6
2030	32	3.6	1.25
2030	32	3.75	1.0

Clearly the TOF-spread performance is affected profoundly by MCP voltage and associated MCP gain, the CFD discrimination values, and the CFD bias voltage. TOF-spreads of order ~1 ns (bottom 2 rows) are unlikely to be achieved for an optimized EPS if, at the same time one requires high efficiency performance. The larger CFD discrimination values (e. g. 32 mV) are likely to be too large to achieve efficient counting. The 2.6 ns value is very encouraging at a very reasonable CFD discrimination value. The actual TOF spread may be a little larger if the full breadth of the entrance aperture is illuminated with the source. However, once full optimization is achieved, it is highly likely that our advertised TOF spread performance of 2.5 to 3.2 ns will be achieved, and probably surpassed.

Table 6.1 EPS Performance Parameters.

Geometric Factor (Instrument Total)		0.074 cm^2 sr
Geometric Factor (Electron Pixel)		0.0062 cm^2 sr
Geometric Factor (Low E Ion Pixel)		0.012 cm2 sr
Geometric Factor (High Energy Ion Pixel)		0.0062 cm^2 sr
Geometric Factor (Diagnostic Ions)		0.0062
Electron Efficiency vs. Energy		Roughly 100% at mid energies. Details in Appendix 8 (TBS 3/1/05)
Low Energy Ion Efficiency vs. En x M		Roughly 20%. Details in Appendix 8 (TBS 3/1/05)
High Energy Ion Efficiency vs En x M		Measured at several percent. Higher values anticipated with tuning, based on Engineering model. Details in Appendix 8 (TBS 3/1/05)
Diagnostic Ion Efficiencies		~100%
Energy Coverage		See Table Below
ΔE / E capability at 50 keV		10 – 15 keV
ΔE / E capability at > 100 keV		10 – 15 keV
Energy / TOF Channel resolution		Electronic Channels in Appendix 8. Primary particle characterisitics TBS 3/1/05
TOF dispersive spread		Demonstrated: 4 ns Expected < 2.5 to 3.2 ns
Mass Species Separation		See Table Below
Angular Coverage (total)		160° x 12°
Angular Coverage (Electrons)		147° x 12°
Angular Coverage (Low Energy Ions)		160° x 12°
Angular Coverage (High Energy Ions)		147° x 12°
Angular Coverage (Diagnostic Ions)		147° x 12°
Angular Pixels (Electrons)		12° x 27° (13° with 13.6° gap)
Angular Pixels (Low Energy Ions)		12° x 30° (full ~27° coverage)
Angular Pixels (High Energy Ions)		12° x 27° (13° with 13.6° gap)
Angular Pixels (Diagnostic Ions)		12° x 27° (13° with 13.6° gap)
Electron Scattering Angle Contrast		Several percent
Collimator Side-Lobes: Position		(Δα, Δβ) = (±28°, ±0°)
Collimator Side-Lobe Fraction/Lobe		~4% per lobe
Energy Coverage:		**Technique**
Electrons	15 keV – 0.6 MeV	Singles / Foil Technique
LE Ions	5 keV – 1 MeV	TOF Only
LE CNO	15 keV – 3 MeV	PH-based mass discrimination may be limited given TOF dispersion
HE Protons	15 keV – 2.8 MeV	TOF vs. Energy
HE He	25 keV – 2.8 MeV	TOF vs. Energy
HE CNO	60 keV – 3 MeV	TOF vs. Energy
Diagnostic Protons	15 keV – 2.8 MeV	Singles
Energy / TOF Channels		Electronic channels in Appendix 8. Primary particle characteristics TBS 3/1/04.

Summary

The engineering model has proven itself to be exceedingly useful for achieving improved understanding of the performance of the EPS instrument. When it is constructed into a fully flight-light configuration,

it will be extensively tested to establish the optimum parameters for trading off such performance characteristics as ion counting efficiencies, TOF performance, anode cross-talk, SSD cross-talk, etc. Here we update Table 4.1 concerning the EPS performance characteristics, making those changes that are appropriate to what we have learned with the calibrations of both the flight EPS and the flight-like engineering model. The few changes from Table 4.1 are indicated in blue.

7.0 Future Plans

Final calibration and characterization of the EPS instrument will require two thrusts: 1) continued characterization and testing of the flight-like engineering model, once completed, and 2) extensive in-flight calibrations.

Engineering Model Plans

The engineering model is essentially complete with a full complement of SSD's (Earlier engineering model tests have used only 2 sets of SSD's) and rimless MCP's. It will then be extensively exercised in a bell jar with radiation sources to find the right set of parameters for optimum efficiency, TOF and Energy measurement performance (MCP voltage, CFD bias, CFD discriminators, Anode discriminators, SSD fast and shaped discriminators, etc.). It will be tested extensively for anode-to-anode and SSD pixel-to-pixel cross-talk. The existences and variations of such cross-talk will be folded into the optimization of the various settings. When the optimization versus parametric settings are well understood, the unit will be moved to the APL accelerator beam chamber for final characterization. In addition, to better characterize the relative efficiencies of different mass species, we will investigate possible cross-talk in the valid-event identification circuitry that may occur when multiple energies and species are measured at the same time.

In-flight Calibration

Described below are the general plans for performing in-flight calibrations, as documented in the previously issued EPS Calibration Plans document (MESSENGER Energetic Particle and Plasma Spectrometer/Energetic Particle Spectrometer (EPPS/EPS) Calibration Plan [7389-9060]). However, given the limited calibrations achieved with the actual flight instrument before delivery, these calibrations have increased in importance. The single most important goal of these in-flight calibrations is to determine the efficiency of ion counting as a function of mass species. This goal is easily achievable for protons. At times the interplanetary environment will be filled with energetic protons of solar origin and energized by interplanetary processes. Since we know that protons dominate such particles, cycling back and forth between the diagnostic ion mode (SSD measurements only) and the full triple-coincident High Energy Ion mode (TOF vs. E) will reveal the counting efficiency of the High Energy Ion Mode for protons. The one modification from the previously published plan is the need for more time (at least 6 months operating within interplanetary space to assure that sufficient intensities of energetic ions are encountered.

Determining the counting efficiency for the heavier ions is not so straightforward. We will rely, in the first instance on scaling according to the dE/dX parameter and scaling from the proton results using calibrations of previously flown TOF-versus-Energy instruments. Figure 31, for example, shows

calibration results for the Galileo Energetic Particle Detector TOF-versus-Energy sensor. Operation of the EPS during the Earth encounter will also be exceedingly valuable because the environment is fairly well cataloged. Earth-environment calibrations of EPS are now included in the official testing plan for the Earth encounter occurring ~1 year after launch. Finally operating EPS in the general environment where other interplanetary assets reside would also be exceedingly valuable, specifically in the vicinity of Earth where such spacecraft as ACE and Wind are operating. Our more general goals for performing in-flight calibrations are documented here.

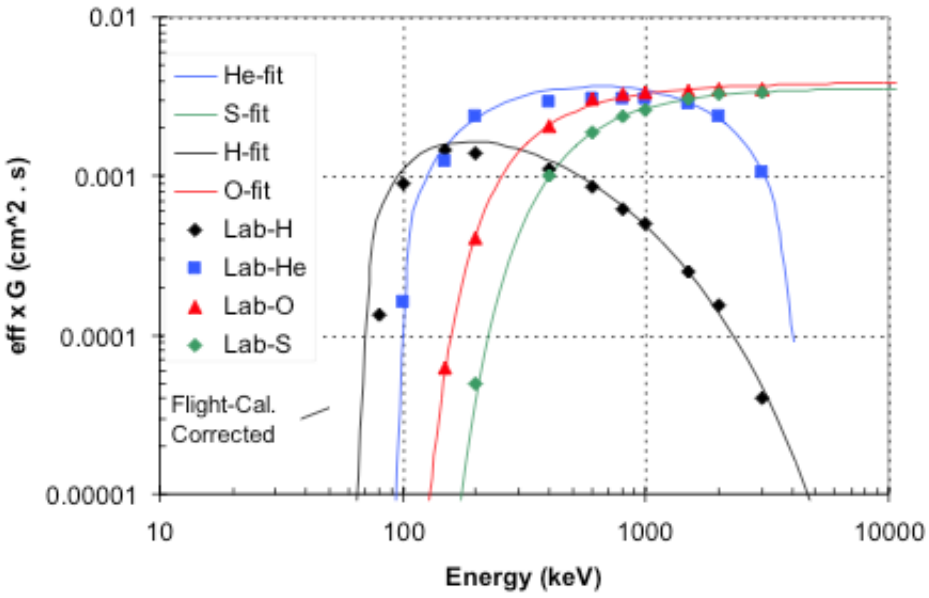

Figure 31. Ion counting efficiency calibrations of the Galileo Energetic Particle Time-of-flight versus Energy sensor. Such previous calibrations will be highly useful in estimating the relative counting efficiencies for protons versus heavier ions.

Interplanetary Space. Energetic particles in interplanetary space will be used to test the mass classification algorithm and verify the content of the various look-up tables. Observations by EPS during the instrument checkout give the first opportunity to cross check the pitch angle magnetic field information with particle signatures. It is therefore important that the magnetometer be operational during the EPPS checkout period. Comparison of particle distribution axes of symmetry with the magnetic field will be attempted with these data to validate the angular response of the instrument. Success will depend on the properties of the energetic particles at the time of observation.

Because the interplanetary environment is variable, it is highly desirable to have the EPS instrument operating substantially longer than that planned for the checkout period. Interplanetary energetic particles tend to vary on the time scale of a solar rotation: 27 days. It would be highly desirable to operate the EPS sensor (with the magnetometer) for a cumulative time period of at least 6 x 27 days prior to the first Mercury flyby in order to optimize the chances of obtaining substantial, calibrating fluxes over the full EPS energy range.

Venus Flybys. The magnetosphere of Venus is characterized by the sporadic appearance of energetic particles. For example, previous missions have observed energetic particle acceleration at the Cytherean bowshock within the upstream solar wind. The EPS sensor will be operated during the Venus fly-by periods to collect and identify energetic particles around the planet. At Venus we will check out operational modes and parameter settings.

Mercury Flybys. The Mercury fly-bys provide the only opportunities prior to the orbital phase of the mission to sample a magnetic field and plasma that are not solar wind or shocked solar wind. The increased degree of ordering provided by the Mercury magnetic field allows superior inter-comparison of magnetometer and particle distribution symmetry axes. The Mercury Fly-bys also offer the best opportunity to carry out dress rehearsals for the orbital phase in terms of operating modes and instrument parametric states.

Calibration Monitoring. In flight, detectors degrade and gains change. Microchannel Plate (MCP) sensor gain changes are monitored by periodic measurements of the pulse height distributions from each of the 7 anodes using built-in capabilities of the instrument. MCP biases can be varied to correct shifts in gain and restore detection efficiency.

Solid State Detector (SSD) performance is monitored using the Time-of-Flight (TOF) versus Energy (E) displays of the Pulse-Height-Analysis event data sampled at all times throughout the mission. Degradations are apparent and quantifiable by noting shifts in the TOF vs. E species tracks. These shifts are normalized to the ground calibration states so that shifts in energy band-passes can be determined and the corresponding look-up table be updated.

8.0 REFERENCES

Agostinelli et al., GEANT4- a simulation toolkit, *NIM(A), 506*, 250-303, 2003.

Andrews, G. B., R. E. Gold, E. P. Keath, D. G. Mitchell, R. W. McEntire, R. L. McNutt, Jr., and N. P. Paschalidis, Compact particle detector for space measurements: prototype performance, *Proc. SPIE Conference 3442*, Missions to the Sun II, 3442, 1998.

Biersack, J. P. and L. Haggmark, *NIM, 174*, 257, 1980.

Frischkorn , H. J., et al., Total yield and escape depth of electrons from heavy ion solid interactions, *IEEE Transactions on Nuclear Science, NS-30*, 1983.

McNutt, Jr., R. L., D. G. Mitchell, E. P. Keath, N. P. Paschalidis, R. E. Gold, and R. W. McEntire, A compact particle detector for low-energy particle measurements, *Proc. SPIE International Symposium, Optical Science, Engineering, and Instrumentation*, Missions to the Sun, 2804, 217-227, 1996.

Appendix 1: EPS Hardware Counters

Address Offset	Rate Counter	Address Offset	Rate Counter	Address Offset	Rate Counter
0x007	Fast 0	0x014	Shaped 1	0x021	Anode 2
0x008	Fast 1	0x015	Shaped 2	0x022	Anode 3
0x009	Fast 2	0x016	Shaped 3	0x023	Anode 4
0x00A	Fast 3	0x017	Shaped 4	0x024	Anode 5
0x00B	Fast 4	0x018	Shaped 5	0x025	Electron Event
0x00C	Fast 5	0x019	Shaped 6	0x026	Ion Event
0x00D	Fast 6	0x01A	Shaped 7	0x027	Start (16 LSBs)
0x00E	Fast 7	0x01B	Shaped 8	0x028	Start (8 LSBs)
0x00F	Fast 8	0x01C	Shaped 9	0x029	Stop (16 LSBs)
0x010	Fast 9	0x01D	Shaped 10	0x02A	Stop (8 MSBs)
0x011	Fast 10	0x01E	Shaped 11	0x02B	Valid TOF (16 LSBs)
0x012	Fast 11	0x01F	Anode 0	0x02C	Valid TOF (8 MSBs)
0x013	Shaped 0	0x020	Anode 1		

Appendix 2. EPS Software Counters.

	Name of software rate counter	Description
1	Electron-count	number of events processed during the accumulation interval
2	High energy ion	number of events processed during the accumulation interval
3	Low energy ion	number of events processed during the accumulation interval
4	Electron Pileup	number of events discarded due to pileup condition
5	Electron Multi-hits	number of events discarded due to multiple hits
6	High energy ion pileup	number of events discarded due to pileup condition
7	High energy multi-hit	number of events discarded due to multiple hits

Appendix 3. EPPS Status Packet Format

Name	Length (bits)	Value	Description
Version	3	000	Designates a source packet
Type	1	0	Designates a telemetry packet
Secondary?	1	1	Secondary header present
ApID	11	010 0000 0101	Application process ID
Grouping	2	11 = None	Grouping flags
Sequence Count	14	Unsigned Integer	Continuous sequence count for each Application Process ID
Length	16	32	Secondary Header + Data (bytes) –1
Secondary Header	32	Unsigned Integer	Time tag (MET)
Status Int.	16	1 – 65535 (0=Off)	Status interval (seconds)
Macro Blocks	16	Unsigned Integer	Number of macro blocks free
TLM Vol	16	Unsigned Integer	Telemetry volume produced (KB)
Watch Addr	16	Unsigned Integer	Memory watch address
Watch Mem	8	Unsigned Integer	Watched memory (pg. no)
Watch Data	2*8	Unsigned Integer	Watched memory
SW Version	8	Unsigned Integer	Software version number
Alarm Id	8		Latest Alarm Id
Alarm Type	1	0 = Persistent 1 = Transient	Latest alarm type
Alarm Count	7	Unsigned Integer	Count of alarms
Cmd Exec	8	Unsigned Integer	Commands executed
Cmd Reject	8	Unsigned Integer	Commands rejected
Mac Exec	8	Unsigned Integer	Macro commands executed
Mac Reject	8	Unsigned Integer	Macro commands rejected
Macro Id	8	Unsigned Integer	Id of most recent macro executed
Macro Learn	1	0 = Not learning 1 = Learning	Macro learn mode
Monitor Response	1	0 = DIS 1 = EN	Monitor response
Write Enb	1	0 = DIS 1 = EN	Memory write enable
spare	5	0	Spare
EPPS Status info	N	variable	EPPS specific status information (see following table)

EPPS Status Information Format

Name	bits	Value	Description
HVPS current	16	integer value	Expansion Bus address 0x006
HVPS voltage	16	integer value	Expansion Bus address 0x008
Bias current	16	integer value	Expansion Bus address 0x00A
Bias voltage	16	integer value	Expansion Bus address 0x00C
EPS status word	16	integer value	Expansion Bus address 0x000
+5 volt monitor	10	log compress 16 to 10 bits	I2C read of LVPS ADC on mux channel 0
-5 volt monitor	10	log compress 16 to 10 bits	I2C read of LVPS ADC on mux channel 1
+12 volt monitor	10	log compress 16 to 10 bits	I2C read of LVPS ADC on mux channel 2
-12 volt monitor	10	log compress 16 to 10 bits	I2C read of LVPS ADC on mux channel 3
+5 current monitor	10	log compress 16 to 10 bits	I2C read of LVPS ADC on mux channel 9
-5 current monitor	10	log compress 16 to 10 bits	I2C read of LVPS ADC on mux channel 10
+12 current monitor	10	log compress 16 to 10 bits	I2C read of LVPS ADC on mux channel 11
-12 current monitor	10	log compress 16 to 10 bits	I2C read of LVPS ADC on mux channel 12
EPS temperature	10	log compress 16 to 10 bits	I2C read of LVPS ADC on mux channel 7
LVPS temperature	10	log compress 16 to 10 bits	I2C read of LVPS ADC on mux channel 13
Primary current monitor	10	log compress 16 to 10 bits	I2C read of LVPS ADC on mux channel 14
Switched primary current monitor	10	log compress 16 to 10 bits	I2C read of LVPS ADC on mux channel 15
15V monitor	10	log compress 16 to 10 bits	FIPS extended address map 93
-15V monitor	10	log compress 16 to 10 bits	FIPS extended address map 94
5V monitor	10	log compress 16 to 10 bits	FIPS extended address map 95
-5V monitor	10	log compress 16 to 10 bits	FIPS extended address map 96
3.5V monitor	10	log compress 16 to 10 bits	FIPS extended address map 97
2.5V monitor	10	log compress 16 to 10 bits	FIPS extended address map 98
FIPS Vref I2C Temp	10	log compress 16 to 10 bits	FIPS extended address map 99
FIPS BH BOT I2C Temp	10	log compress 16 to 10 bits	FIPS extended address map 9a
FIPS BH TOP I2C Temp	10	log compress 16 to 10 bits	FIPS extended address map 9b
FIPS DS-HV I2C Temp	10	log compress 16 to 10 bits	FIPS extended address map 9c
MCP-HV monitor	10	log compress 16 to 10 bits	FIPS extended address map 9d
PA-HV monitor	10	log compress 16 to 10 bits	FIPS extended address map 9e
DSHV Monitor	10	log compress 16 to 10 bits	FIPS extended address map 9f
DSHV Step	10	log compress 16 to 10 bits	Step at which HV values were sampled
FIPS BH BOT Temp	10	log compress 16 to 10 bits	I2C read of LVPS ADC on mux channel 6
FIPS BH TOP Temp	10	log compress 16 to 10 bits	I2C read of LVPS ADC on mux channel 8
Spare	8	zero-filled	Pads to next word boundary
I2C read command address	16	I2C read address	Software (upper byte = 0xe for extended read address, 8 LSBs = read address)
I2C read command result	16	16-bit integer	Software

Appendix 4. EPS High-Priority Data

Table 1. N1 Science Data Telemetry Packet Format (after fast decompression)

Name	Length (bits)	Value	Description
Version	3	000	Designates a source packet
Type	1	0	Designates a telemetry packet
Secondary?	1	1	Secondary header is present
App ID	11	010 0001 0001	EPPS
Grouping	2	11 = None	Grouping flags
Sequence Count	14	Unsigned integer	Continuous sequence count for each Application Process ID
Length	16	3 – 4099	Packet length (bytes) - 1
Secondary Header	32	Unsigned integer	Time tag (MET)
High Energy Ions for detector s 0-5	6*352= 2112	10-bit log compressed values within 16-bit words	22 words (16 bits each) per detector. Each word contains a 10-bit log compressed count accumulated over N1 seconds (132 words total). In Diagnostic Mode. First 8 words are Ion energy spectrum. The rest are all zeros.
Electron (coarse) for detectors 0-5	6*128=768	10-bit log compressed values within 16-bit words	Eight 16-bit words per detector. Each word contains a 10-bit log compressed count accumulated over N1 seconds (48 words total)
Electron (fine) for detectors 0-5 (see note below)	6*32*10= 1920	10-bit log compressed values within 16-bit words	Two 16-bit words per detector corresponding to a 12-word set. A separate 12-word set is reported for each of the ten N1/10 second subintervals. Each 16-bit word contains a 10-bit log compressed value. (120 words total)
Low Energy Ion (TOF only) for detectors 0-5	6*256 = 1536	10-bit log compressed values within 16-bit words	Sixteen 16-bit words per detector. Each word contains a 10-bit log compressed count accumulated over N1 seconds. (96 words total) All zeros in Diagnostic Mode.
Rate Channel counter & Software Rates	42*16=672	10-bit log compressed values within 16-bit words	35 Hardware rate counters and 7 software rate counters accumulated of N1 seconds and each counter is log compressed to 10 bits and stored within a 16-bit word (42 words total)
Housekeeping	528	16 bit values	33 words of housekeeping data recorded over N1 seconds (see table 2)
PHA	768 to 1344	Up to ten sets of values (64 to 112 bits each)	Up to 10 PHA events (varying in size from 4 to 7 words) acquired over N1 seconds

Table 2. EPPS housekeeping values contained in High Priority Telemetry Packet

1	HVPS setting
2	Bias setting
3	TOF anode 0 disc setting
4	TOF anode 1 disc setting
5	TOF anode 2 disc setting
6	TOF anode 3 disc setting
7	TOF anode 4 disc setting
8	TOF anode 5 disc setting
9	TOF Start CFD setting
10	TOF Stop CFD setting
11	Heavy-0 Disc setting
12	Heavy-1 Disc setting
13	Ion Fast channels 1, 3, 5
14	Ion Shaped channels 1, 3, 5
15	Ion Fast channels 7, 9, 11
16	Ion Shaped channels 7, 9, 11
17	Electron Fast Channels 0, 2, 4
18	Electron Shaped Channels 0, 2, 4
19	Electron Fast Channels 6, 8, 10
20	Electron Shaped Channels 6, 8, 10
21	Command word A mirror
22	Command word B mirror
23	Event parameter A mirror
24	Event parameter B mirror
25	Event parameter C mirror
26	HVPS clock adjust value
27	Bias clock adjust value
28	LVPS Control word
29	Invalid channel ID count
30	EPS-fifo-reset count
31	I2C Bus error count
32	Value provided by most recent bus read command
33	Spare

For the “Fine” electron data, super bin 0 is sum of bin 0 to bin 3, while Super bin 1 is the sumfrom bin 4 to bin 7. The subset is fixed.

Appendix 5. EPS Medium-Priority Data

N2 Science Data Telemetry Packet Format (after fast decompression)

Name	Length (bits)	Value	Description
Version	3	000	Designates a source packet
Type	1	0	Designates a telemetry packet
Secondary?	1	1	Secondary header is present
App ID	11	010 0001 0010	EPPS
Grouping	2	01 = First 00 = Continuation 10 = Last 11 = None	Grouping flags
Sequence Count	14	Unsigned integer	Continuous sequence count for each Application Process ID
Length	16	3 - 4099	Packet length (bytes) – 1
Secondary Header	32	Unsigned integer	Time tag (MET)
High Energy Ion	1152	10-bit log compressed values	Twelve 16-bit words per detector. Each word contains a 10-bit log compress matrix box accumulated over N2 seconds (72 words total).). In Diagnostic Mode. First 8 words are Ion energy spectrum. The rest are all zeros.
Electron (coarse)	768	10-bit log compressed values	Eight 16-bit words per detector. Each word contains a 10-bit log compress matrix box accumulated over N2 seconds (48 words total)
Electron (fine). (See note Appendix 4)	1920	10-bit log compressed values	Two 16-bit words per detector. Each word contains a 10-bit log compressed super box accumulated over 10 subintervals of N2/10 seconds (120 words total)
Low Energy Ion (TOF only)	768	10-bit log compressed values	Eight 16-bit words per detector. Each word contains a 10-bit log compressed histogram box accumulated over N2 seconds. (48 words total). All zeros in Diagnostic Mode.
Rate Channel counter & Software Rates	384	10-bit log compressed values	17 Hardware rate counters and 7software rate counters accumulated over N2 seconds. Each counter is log compressed to 10-bits and stored within a 16-bit word. (24 words total)
PHA	0 to 2240	Up to twenty variable sized PHA events	Up to 20 PHA events (varying in size from 4 to 7 words) acquired over N2 seconds (80 to 140 words total)

The specific 17 counters will be command-able through a table upload.
Currently the default counters are:

12 Shaped counters
Electron Event
Ion Event
Start
Stop
Valid TOF

Appendix 6. EPS Low-Priority Data

Low Priority Science Data Telemetry Packet Format (after fast decompression)

Name	Length (bits)	Value	Description
Version	3	000	Designates a source packet
Type	1	0	Designates a telemetry packet
Secondary?	1	1	Secondary header is present
App ID	11	010 0001 0011	EPPS
Grouping	2	11 = None	Grouping flags
Sequence Count	14	Unsigned integer	Continuous sequence count for each Application Process ID
Length	16	3 - 4099	Packet length (bytes) - 1
Secondary Header	32	Unsigned integer	Time tag (MET)
N PHA Events	0 to 33600	N unsigned integers	Up to 300 PHA Events (varying in size from 4 to 7 words) (0 to 2100 words)

The actual number of words in each PHA event depends on the event type.

Appendix 7. Pulse Height Analysis Telemetry Data Formats

word 0	(0x03) EPS Electron PHA Event Short ID (8 bits)					
word 1	Energy Peak (8 LSBs)					
word 2	Energy Baseline (8 LSBs)					
word 3	Energy Peak (4 MSBs)				Energy Baseline (4 MSBs)	
word 4	0	0	0	0	Multiple	Electron Channel (3 bits)

word 0	(0x01) EPS Low Energy Ion PHA Event Short ID (8 bits)					
word 1	TOF (8 LSB)					
word 2	0	0	0	Heavy Disc 1	Heavy Disc 0	TOF (3 MSB)
word 3	0	0	Start Segment 6 bits			

Word 0	(0x05) EPS High Energy Ion PHA Event Short ID (8 bits)			
Word 1	Energy Peak (8 LSBs)			
Word 2	Energy Baseline (8 LSBs)			
Word 3	Energy Peak (4 MSBs)		Energy Baseline (4 MSBs)	
Word 4	TOF (8 LSBs)			
Word 5		Mulitple	Ion Channel (3 bits)	TOF (3 MSBs)
Word 6	Heavy Disc-1	Heavy Disc-0	Start Segment (6 bits)	

word 0	(0x0B) EPS Diagnostic Event PHA Event Short ID (8 bits)					
word 1	Energy Peak (8 LSBs)					
word 2	Energy Baseline (8 LSBs)					
word 3	Energy Peak (4 MSBs)				Energy Baseline (4 MSBs)	
word 4	0	Heavy Disc-1	Heavy Disc-0	Multiple	Ion fired	Ion or Electron Channel (3 bits)
word 5	0	0	Start Segment (6 bits)			

Appendix 8. Channel Definitions (Missing Table entries to be supplied by 3/1/05)

Electron Channels (Nominal Parameters)

Channel	E1 (elect)	E2(elect)	E1(in)	E2(in)	Eff-1	Eff-2
	keV	keV	keV	keV	fraction	fraction
1	0	25				
2	25	39				
3	39	60				
4	60	94				
5	94	146				
6	146	227				
7	227	352				
8	352	547				

Notes: "elect" refers to energy deposited in the SSD and read out by the electronics. The "in" parameters are the mean input energies, taking into account energy losses and scattering. "Eff" is efficiency. Eff-1 and Eff-2 are efficiencies at the end-point energies. The "in" parameters and the "efficiency" is calculated using GEANT-4

Low Energy Ion Channels (Nominal Parameter) (Exact Organization TBS 3/1/05)

Channel	Species	TOF_1	TOF_2	E1	E2	Eff-1	Eff-2
	L, M, H	ns	ns	Hy or O	Hy or O	fraction	fraction
1	L	0	1.1				
2	L	1.1	7.5				
3	L	7.5	40.5				
4	L	40.5	215				
5	L	215					
6	M	0	1.1				
7	M	1.1	7.5				
8	M	7.5	40.5				
9	M	40.5	215				
10	M	215					
11	M	0	1.1				
12	H	1.1	7.5				
13	H	7.5	40.5				
14	H	40.5	215				
15	H	215					
16							

Notes: "L, M, H" refers to light ions, medium ions, and heavy ions, based on the range of pulse-height settings: L = noise threshold to H-0 discriminator, M = H-0 to H-1 discriminator, and H = > H-1 discriminator. For calculation of E1 and E1, it is assumed that L = Hydrogen and H = Oxygen. Eff-1 and Eff-2 are efficiencies at the end points calculated assuming that a 100 keV proton generates a 0.75 electrons from a foil, and then scaling with dE/dX.

High Energy Ions (Nominal Parameters): See Figure at end of Appendix 8

Channel	Species	E1(el)	E2(el)	E1(in)	E2(in)	Effi-1	Eff-2
		keV	keV	keV	keV	fraction	fraction
0	BG						
1	P		,28				
2	P	28	68				
3	P	68	164				
4	P	164	396				
5	P	958	2316				
6	P	>2316					
7	He	28	164				
8	He	164	958				
9	He	>958					
10	Heavy		<28				
11	Heavy	28	81				
12	Heavy	81	233				
13	Heav-L	233	673				
14	Heav-M	233	673				
15	Heav-H	233	673				
16	Heav-L	673	1941				
17	Heav-M	673	1941				
18	Heav-H	>1941					
19	Heav-L	>1941					
20	Heav-H	>1941					
21	BG						

Notes: E1(el) and E2(el) is electronic energy read out from SSD. TOF information is contained here only in the identification of the species. The E1(in) and E2(in) is the input energy as calculated with SRIM. Efficiency is based on dE/dX scaling from protons.

Ion Diagnostic Channels (Nominal Parameters)

Channel	E1 (elect)	E2(elect)	E1(in)	E2(in)	Eff-1	Eff-2
	keV	keV	keV	keV	fraction	fraction
1	0	25			1	1
2	25	39			1	1
3	39	60			1	1
4	60	94			1	1
5	94	146			1	1
6	146	227			1	1
7	227	352			1	1
8	352	547			1	1

Notes: "elect" refers to energy deposited in the SSD and read out by the electronics. The "in" parameters are the mean input energies, taking into account energy losses and scattering.

High Energy Ions Notional Channels

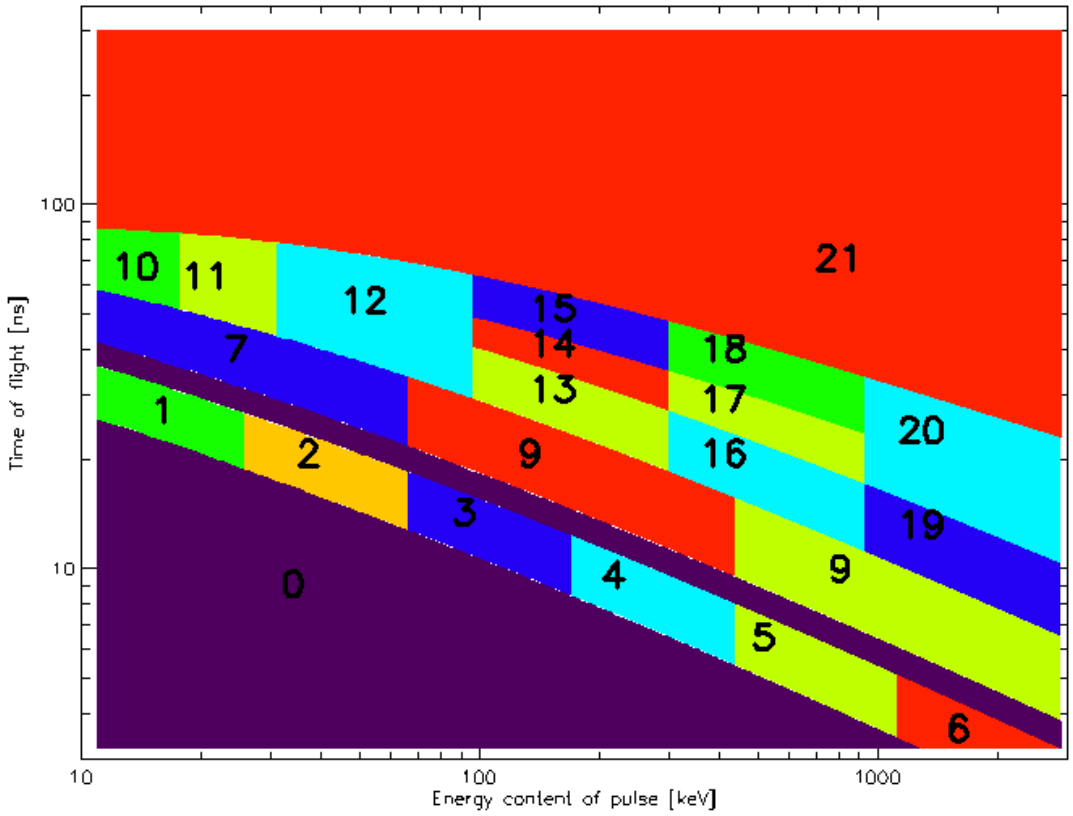

Appendix 9. The JHU/APL Calibration Facility

Calibration of the EPS instrument was conducted at the JHU/APL instrument testing facility through a combination of long-duration, radiation-source exposures (Am-241 degraded alpha source) and discrete exposures from our 170 kV particle accelerator system. The Air Insulated Accelerator, obtained from Peabody Scientific, is a versatile system capable of producing a broad range of ion species to energies of 170 keV. The accelerator incorporates a number of features that result in reliable, easy operation.

The system includes a Duoplasmatron Ion source, extraction gap, Einzel Lens and Wien filter mounted in the insulated terminal structure along with all associated power supplies. A large diameter accelerator tube accelerates the beam to it's final energy. Within the accelerator tube is an electrostatic bi-potential lens that is used to focus the beam to its final size at the target position.

The system will produce beams of H, O, and noble gas ions with intensities over the range of 100's to 1,000,000 particles/cm^2/sec at the target position in an energy range of 3 keV to 170 keV.

Typical operation of the system is as follows. Ions are formed in the ion source and are extracted to energies of up to 20 keV by the extraction gap. The high-brightness, divergent beam is then focused by

the terminal Einzel lens through the mass analysis system to a focus at the entrance to the accelerator tube. The accelerator tube provides additional acceleration up to the maximum beam energy, or deceleration to minimum beam energy. The beam is focused by an electro-static lens to an appropriate size at the target position.

The Duoplasmatron is a low pressure arc discharge source in which the gas to be ionized is electrostatically constricted by a funnel-shaped intermediate electrode placed between the filament and the anode. A strong axial magnetic field is developed between the intermediate electrode and the anode, which further constricts the discharge to a narrow plasma beam along the axis of the exit aperture.

The optical quality of the beam depends upon the extraction region of the source-lens combination. The Duoplasmatron source and extraction gap are designed to operate as a unit and optimize the efficiency of this Pierce-extraction region. The lens insulators are optically shielded from the ion beam to prevent surface charging or contamination from the vacuum system. This prevents the formation of a spark tracks on the insulators which lead to lens voltage breakdown. The extraction electrode is made from copper for good heat conduction and is nickel-plated to prevent corrosion. It is liquid cooled by a cooling line external to the vacuum thus eliminating any possible leakage in the vacuum. The divergence of the beam from the ion source is related to the extraction geometry and extraction voltage. The gap geometry provides a strong electric field region to extract ions efficiently from the source plasma, resulting in a superior quality beam.

The Einzel lens is a three-element electrostatic cylindrical tube lens with the center electrode elevated near to source potential. Operated in this manner, the lens is a classical saddle point Einzel lens which decelerates the divergent beam from the source and extraction gap and then reaccelerates it back to the extraction energy. The result is a strong focusing action. The focal length is determined by the voltage applied to the center electrode.

The terminal structure is a strong, rigid welded frame that supports the ion source components at high voltage. The terminal has a smooth, four-inch radius outer shell that provides equipotential control of the high voltage. This design prevents corona discharge and results in highly stable voltage operation.

Appendix 10. Calibration Runs Listing

Table A10.1 groups several accelerator calibration runs when the EPS instrument was in a flight configuration, including the collimmator. A total of 26 discreet runs are reported here along with the date and EST of each run. The Accelerator Parameter – Energy lists the energy of the ion incident on the EPS instrument in keV (20 keV extraction voltage + post acceleration voltage = Energy). The Accelerator Parameter – ExB is the actual accelerator setting of the Wien Filter used to select the desired species, the intended species is also listed. Which of the 6 EPS detectors and associated time of flight (TOF) Anode is listed. The Discriminator setting for both the Ion Fast and Ion Shaped channels is listed. The setting for the High Voltage Power Supply (HVPS) and Solid State Detector (SSD) bias is listed, as well as the settings for the TOF Anode, TOF Start constant fraction discriminator (CDF), TOF Stop CDF, and both Heavy Ion Discriminators. The next group represents the counts observed during the run as a function of instrument cycle. The count rate of the Starts, Stops, Valid TOF, and Ion Events

(triples) is listed as well as the count rate observed on SSD from the Shaped, and Fast systems. The count rate on the associated anode is also listed.

The group of values that begin with the word “analyzed” represent analyses of the reported energy and TOF peak and full width at half of the maximum (FWHM) given in bin number. Comments about the analyses are also shown. The group labeled “Main Spectra” is to indicate, for those runs with multiple peaks, which of those were used in the overall calibration spectra.

Table 10.1

Run #	1	2	3	4	5	6	7	8	8	8	9	9	9	9
Date	09/23	09/23	09/23	09/23	09/23	09/24	09/24	09/26	09/26	09/26	09/26	09/26	09/26	09/26
Time	2025-2040	2126-2140	2205-2220	2256-2311	2344-2400	0031-0045	0118-0128	1420-1440	1420-1440	1420-1440	1903-1918	1903-1918	1903-1918	1903-1918
Accelerator Paramter - Energy	80	95	110	125	140	155	170	170	170	170	170	170	170	170
Accelerator Paramter - ExB	510	510	510	510	510	510	510	128	128	128	332	332	332	332
Intended Species	protons	protons	protons	protons	protons	protons	protons	oxygen	oxygen	oxygen	helium	helium	helium	helium
Accelerator Target SSD - N	5	5	5	5	5	5	5	5	5	5	5	5	5	5
Accelerator Target Anode- M	3	3	3	3	3	3	3	3	3	3	3	3	3	3
Ion Fast Channels Disc	275	275	275	275	275	275	275	250	250	250	250	250	250	250
Ion Shaped Channels Disc	325	325	325	325	325	325	325	250	250	250	250	250	250	250
HVPS setting	201	201	201	201	201	201	201	189	189	189	197	197	197	197
Bias setting	190	190	190	190	190	190	190	190	190	190	190	190	190	190
TOF Anode M Disc setting	184	184	184	184	184	184	184	184	184	184	184	184	184	184
TOF Start CFD setting	100	90	90	90	90	90	90	100	100	100	80	80	80	80
TOF Stop CFD setting	100	110	110	110	110	110	110	100	100	100	95	95	95	95
Heavy-0 Disc	184	184	184	184	184	184	184	184	184	184	184	184	184	184
Heavy-1 Disc	184	184	184	184	184	184	184	184	184	184	184	184	184	184
Data Collection Mode														
Starts	7552	12032	11008	12800	11520	12544	17408	12032	12032	12032	33792	33792	33792	33792
Stops	47104	75776	31744	92160	10240	10496	59392	52224	52224	52224	65536	65536	65536	65536
Valid TOF	336	328	264	432	240	296	1120	1056	1056	1056	784	784	784	784
Ion Event	25	57	45	108	56	100	432	48	48	48	124	124	124	124
N-SSD Shaped Counts	24576	64512	28160	83968	8064	8704	57344	5376	5376	5376	36864	36864	36864	36864
N-SSD Fast Counts	32256	67584	28160	86016	7552	8192	59392	8448	8448	8448	37888	37888	37888	37888
M-Anode Counts	92	172	92	196	114	112	328	344	344	344	400	400	400	400
EPS Temperature	-3.18364	-3.18364	-3.1836	-3.18364	-3.18364	-3.18364	-3.18364	-3.18364	-3.18364	-3.18364	-3.18364	-3.18364	-3.18364	-3.18364
Efficiency - TOF (%)	1.04167	0.485322	0.9375	0.502232	3.177966	3.613281	1.88578	12.5	12.5	12.5	2.069257	2.06926	2.069257	2.06926
Efficiency - E.v.TOF (%)	0.0775	0.084339	0.1598	0.125558	0.741525	1.220703	0.72737	0.568182	0.568182	0.568182	0.32726	0.32728	0.32726	0.32728
Analyzed Energy	72	88.5	109	129	154	178.1	200.9	56.7	56.7	56.7	72.1	148	72.1	148
Analyzed Energy fwhm	18.2	21.3	21.6	22.9	22.3	20.1	21	20.4	20.4	20.4	14.3	17.6	14.3	17.6
Analyzed tof	103.6	95.6	89	83.4	76.9	73.1	69.7	216.8	48.2	286.9	32.8	32.8	90.8	90.8
Analyzed tof fwhm	28.5	26.2	25.9	28.3	26.2	26.9	25.2	56.2	85.3	47.1	39.3	39.3	49	49
Comments-1	single peak	single peak	single peak	single peak	single peak	single peak	single peak	main tof	first tof	last tof	Main Energy first TOF	Second Energy first TOF	Main Energy second TOF	Second Energy second TOF
Main Spectra?	x	x	x	x	x	x	x	x					x	
Comments-2														

10	10	10	11	11	11	11	12	13	13	13	13	13	13	14	14	15
09/26	09/26	09/26	09/26	09/26	09/26	09/26	09/26	09/26	09/26	09/26	09/26	09/26	09/26	09/27	09/27	09/27
2014-2028	2014-2028	2014-2028	2226-2241	2226-2241	2226-2241	2226-2241	2307-2323	2344-2359	2344-2359	2344-2359	2344-2359	2344-2359	2344-2359	0011-0024	0011-0024	0147-0200
170	170	170	155	155	155	155	96	95	95	95	95	95	95	95	95	110
128	128	128	510	510	510	510	503	367	367	367	367	367	367	302	302	508
oxygen	oxygen	oxygen	protons	protons	protons	protons	protons	Helium	Helium	Helium	Helium	Helium	Helium	Helium	Helium	Protons
5	5	5	5	5	5	5	5	5	5	5	5	5	5	5	5	5
3	3	3	3	3	3	3	3	3	3	3	3	3	3	3	3	3
250	250	250	250	250	250	250	250	250	250	250	250	250	250	250	250	250
250	250	250	250	250	250	250	250	250	250	250	250	250	250	250	250	250
197	197	197	197	197	197	197	197	197	197	197	197	197	197	197	197	197
190	190	190	190	190	190	190	190	190	190	190	190	190	190	190	190	190
184	184	184	184	184	184	184	184	184	184	184	184	184	184	184	184	184
80	80	80	80	80	80	80	80	80	80	80	80	80	80	80	80	80
95	95	95	95	95	95	95	96	95	95	95	95	95	95	95	95	95
184	184	184	184	184	184	184	184	184	184	184	184	184	184	184	184	184
184	184	184	184	184	184	184	184	184	184	184	184	184	184	184	184	184
442368	442368	442368	94208	94208	94208	94208	48128	98304	98304	98304	98304	98304	98304	393216	393216	104448
704512	704512	704512	124928	124928	124928	124928	34816	126976	126976	126976	126976	126976	126976	1835008	1835008	81920
67584	67584	67584	5248	5248	5248	5248	992	3904	3904	3904	3904	3904	3904	98304	98304	3136
4352	4352	4352	92	92	92	92	28	26	26	26	26	26	26	576	576	48
52224	52224	52224	30208	30208	30208	30208	10240	9472	9472	9472	9472	9472	9472	30208	30208	18432
88064	88064	88064	32256	32256	32256	32256	10240	20480	20480	20480	20480	20480	20480	81920	81920	18944
16896	16896	16896	5248	5248	5248	5248	1472	4480	4480	4480	4480	4480	4480	20992	20992	5248
-3.18364	-3.18364	-3.18364	-3.18364	-3.18364	-3.18364	-3.18364	-3.18364	-3.18364	-3.18364	-3.18364	-3.18364	-3.18364	-3.18364	-3.18364	-3.18364	-3.18364
76.74419	76.74419	76.74419	16.26984	16.26984	16.26984	16.26984	9.6875	19.0625	19.0625	19.0625	19.0625	19.0625	19.0625	120	120	16.55405
4.94186	4.94186	4.94186	0.285218	0.285218	0.285218	0.285218	0.273438	0.126953	0.126953	0.126953	0.126953	0.126953	0.126953	0.703125	0.703125	0.253378
59.3	59.3	59.3	55.3	178.4	55.3	178.4	90.1	58.6	30	87.9	58.6	30	87.9	41.8	41.8	110.1
26.2	26.2	26.2	20.6	12	20.6	12	10.9	13.6	15.9	17.1	13.6	15.9	17.1	44.6	44.6	11.9
207.3	43	287.5	210.9	210.9	294.5	294.5	98.7	117.5	117.5	117.5	32.3	32.3	32.3	142.3	51.5	92.9
60.9	91.1	49.4	60.6	60.6	76.4	76.4	34.5	54	54	54	54.9	54.9	54.9	52	52.8	51.5
Main TOF x	first TOF	last TOF	first energy main TOF x	second energy main TOF	first energy crappy second tof	second energy poor second tof	single	Main Energy main TOF x	first energy main TOF	last energy main TOF	Main Energy first TOF	first energy first tof	last energy first tof	main TOF x	first tof	single x
Helium	Protons?	Oxygen	Helium	cant be protons, not on track												

FSCM NO.	SIZE	DRAWING NO.	REV.
88898	A	7384-9471	A
SCALE	DO NOT SCALE PRINT	SHEET 63 of 65	

Table 10.1 Continued

16	16	16	16	16	16	17	17	18	19	19	19	19	20	20	20	20
09/27 0212-0226	09/27 0212-0226	09/27 0212-0226	09/27 0212-0226	09/27 0212-0226	09/27 0212-0226	09/27 0233-0247	09/27 0233-0247	09/27 0350-0400	09/27 0418-0429	09/27 0418-0429	09/27 0418-0429	09/27 0418-0429	09/27 0435-0446	09/27 0435-0446	09/27 0435-0446	09/27 0435-0446
110	110	110	110	110	110	110	110	120	120	120	120	120	120	120	120	120
369	369	369	369	369	369	305	305	510	369	369	369	369	308	308	308	308
Helium	Helium	Helium	Helium	Helium	Helium	helium	helium	proton	helium	helium	helium	helium	helium	helium	helium	helium
5	5	5	5	5	5	5	5	5	5	5	5	5	5	5	5	5
3	3	3	3	3	3	3	3	3	3	3	3	3	3	3	3	3
250	250	250	250	250	250	250	250	250	250	250	250	250	250	250	250	250
250	250	250	250	250	250	250	250	250	250	250	250	250	250	250	250	250
197	197	197	197	197	197	197	197	197	197	197	197	197	197	197	197	197
190	190	190	190	190	190	190	190	190	190	190	190	190	190	190	190	190
184	184	184	184	184	184	184	184	184	184	184	184	184	184	184	184	184
80	80	80	80	80	80	80	80	80	80	80	80	80	80	80	80	80
95	95	95	95	95	95	95	95	95	95	95	95	95	95	95	95	95
184	184	184	184	184	184	184	184	184	184	184	184	184	184	184	184	184
184	184	184	184	184	184	184	184	184	184	184	184	184	184	184	184	184
147456	147456	147456	147456	147456	147456	208896	208896	176128	901120	901120	901120	901120	143360	143360	143360	143360
294912	294912	294912	294912	294912	294912	901120	901120	163840	770048	770048	770048	770048	237568	237568	237568	237568
8192	8192	8192	8192	8192	8192	43008	43008	7936	41984	41984	41984	41984	10752	10752	10752	10752
160	160	160	160	160	160	416	416	212	832	832	832	832	360	360	360	360
43008	43008	43008	43008	43008	43008	29184	29184	33792	54272	54272	54272	54272	26624	26624	26624	26624
114688	114688	114688	114688	114688	114688	98304	98304	34816	83968	83968	83968	83968	49152	49152	49152	49152
7808	7808	7808	7808	7808	7808	12032	12032	11264	60416	60416	60416	60416	8448	8448	8448	8448
-3.18364	-3.18364	-3.18364	-3.18364	-3.18364	-3.18364	-3.18364	-3.18364	-3.18364	-3.18364	-3.18364	-3.18364	-3.18364	-3.18364	-3.18364	-3.18364	-3.18364
7.142857	7.142857	7.142857	7.142857	7.142857	7.142857	43.75	43.75	22.79412	50	50	50	50	21.875	21.875	21.875	21.875
0.139509	0.139509	0.139509	0.139509	0.139509	0.139509	0.423177	0.423177	0.608915	0.990854	0.990854	0.990854	0.990854	0.732422	0.732422	0.732422	0.732422
72.3	37.5	145.3	72.3	37.5	145.3	45.8	45.8	155.1	54.3	107.5	54.3	107.5	54.7	32.9	80.1	54.7
16	11.9	20.9	16	11.9	20.9	45.2	45.2	12.5	11.3	17	11.3	17	12.5	24.4	21.7	12.5
106.1	106.1	106.1	30.9	30.9	30.9	130.3	47.3	82.4	108	108	19.4	19.4	113.7	113.7	113.7	40.6
65.3	65.3	65.3	55.5	55.5	55.5	38.9	41.6	45.8	83.1	83.1	64	64	38.5	38.5	38.5	34.4
Main Energy main TOF x	first energy main TOF	last energy main TOF	Main Energy first TOF	first energy first tof	last energy first tof	Main Energy main TOF x	Main Energy first TOF	single x	first peak main tof	second peak main tof x	first peak first tof	second peak first tof	Main Energy main TOF x	first energy main TOF	last energy main TOF	Main Energy first TOF
note that the first energy peak is substantial as well										note that first peak is substantial as well						

20	20	21	21	22	22	23	23	24	24	25	25	26	26
09/27 0435-0446	09/27 0435-0446	09/27 0452-0502	09/27 0452-0502	09/28 1243-1300	09/28 1243-1300	09/28 1310-1326	09/28 1310-1326	09/28 1330-1419	09/28 1330-1419	09/28 1422-1443	09/28 1422-1443	09/28 1500-1558	09/28 1500-1558
120	120	120	120	170	170	155	155	140	140	125	125	110	110
308	308	128	128	113	113	139	139	127	127	127	127	120	120
helium	helium	oxygen	oxygen	oxygen	oxygen	oxygen	oxygen	oxygen	oxygen	oxygen	oxygen	oxygen	oxygen
5	5	5	5	5	5	5	5	5	5	5	5	5	5
3	3	3	3	3	3	3	3	3	3	3	3	3	3
250	250	250	250	250	250	250	250	250	250	250	250	200	200
250	250	250	250	250	250	250	250	250	250	250	250	200	200
197	197	197	197	206	206	206	206	206	206	206	206	206	206
190	190	190	190	190	190	190	190	190	190	190	190	190	190
184	184	184	184	184	184	184	184	184	184	184	184	184	184
80	80	80	80	120	120	120	120	120	120	120	120	120	120
95	95	95	95	120	120	120	120	120	120	120	120	120	120
184	184	184	184	184	184	184	184	184	184	184	184	184	184
184	184	184	184	184	184	184	184	184	184	184	184	184	184
143360	143360	966656	966656	43008	43008	79872	79872	106496	106496	491520	491520	233472	233472
237568	237568	1146880	1146880	65536	65536	131072	131072	155648	155648	524288	524288	217088	217088
10752	10752	112640	112640	3456	3456	14592	14592	15104	15104	65536	65536	23040	23040
360	360	1152	1152	126	126	752	752	148	148	192	192	28	28
26624	26624	21504	21504	6016	6016	12544	12544	3456	3456	4224	4224	1248	1248
49152	49152	69632	69632	10240	10240	22016	22016	15616	15616	29696	29696	12800	12800
8448	8448	58368	58368	5248	5248	13568	13568	18432	18432	81920	81920	39936	39936
-3.18364	-3.18364	-3.18364	-3.18364	-3.18364	-3.18364	-3.18364	-3.18364	-3.18364	-3.18364	-3.18364	-3.18364	-3.18364	-3.18364
21.875	21.875	161.7647	161.7647	33.75	33.75	66.27907	66.27907	96.72131	96.72131	220.6897	220.6897	180	180
0.732422	0.732422	1.654412	1.654412	1.230469	1.230469	3.415898	3.415898	0.947746	0.947746	0.646552	0.646552	0.21875	0.21875
32.9	80.1	47.2	47.2	56.6	56.6	55.1	55.1	48	48	40	40	30	30
24.4	21.7	32.5	32.5	22.2	22.2	22.2	22.2	21.4	21.4	29.4	29.4	26.3	26.3
40.6	40.6	228.6	305.7	210.2	296.5	206.2	277.2	223.9	303.4	241.1	326.6	250.2	346.7
34.4	34.4	79.2	91.5	37.6	60.8	31.6	46.9	44	51.6	68.4	50.5	81.4	73.2
first energy first tof	last energy first tof	main tof x	last tof	main tof x	last tof	main tof x	last tof	main tof x	last tof	main tof x	last tof	main tof x	last tof
		last tof may be oxygen peak		last tof may be oxygen peak		last tof may be oxygen peak		last tof may be oxygen peak		last tof may be oxygen peak		last tof may be oxygen peak	

FSCM NO.	SIZE	DRAWING NO.	REV.
88898	A	7384-9471	A
SCALE	DO NOT SCALE PRINT	SHEET 64 of 65	

Appendix 11. Data ApIDs and Data Rates

Here is a list of the ApIDs, and other interesting info related to them, organized by FILE priority:

High-Priority Data
(1) ApID 211 (hex) - EPS High-Priority Science, typical integration interval = 300 seconds, typical size (compressed) = 373 bytes
(2) ApID 221 or 225 or 229 or 22D (hex), - FIPS High-Priority Science, typical integration interval = 600 seconds, typical size (compressed) = 872 bytes. Note: there are four ApIDs listed, but only one type is output at any given time. The different ApIDs reflect different operating modes that FIPS will be in.
(3) ApID 205 (hex) - EPPS status packet, 10-second integration interval, typical size = 80 bytes. Note: This packet is output every 10 seconds, but we want to put only one out of every 120 in the high priority file. The rest should go into contingency.

Medium-Priority Data
(1) ApID 212 (hex) - EPS Medium-Priority Science, typical integration interval = 30 seconds, typical size (compressed) = 304 bytes
(2) ApID 222 or 226 or 22A or 22E (hex), - FIPS Medium Priority Science, typical integration interval = 60 seconds, typical size (compressed) = 550 bytes. Note: there are four apIDs listed, but only one type is output at any given time. The different ApIDs reflect different operating modes that FIPS will be in.

Low-Priority Data
(1) ApID 213 (hex) - EPS Low Priority Science, typical integration interval = 300 seconds, typical size (compressed) = 600 bytes
(2) ApID 223 or 227 or 22B or 22F (hex), - FIPS Low Priority Science, typical integration interval = ~~600~~ 60 seconds, typical size (compressed) = 430 bytes. Note: there are four ApIDs listed, but only one type is output at any given time. The different ApIDs reflect different operating modes that FIPS will be in.

Contingency Data
(1) ApID 205 (hex) - EPPS status packet, 10-second integration interval, typical size = 80 bytes. Note: This packet is output every 10 seconds, but we want to put 119 out of every 120 in the contingency file. Every 120th packet should go in the high priority file.

Assumptions for the above numbers: FAST compression gives 3 to 1 compression, PHA slots mostly filled, FIPS burst mode not used.

This gives the following BYTE rates for the various priorities:
High = 2.76 bytes per second
Medium = 19.3 bytes per second
Low = 2.71 bytes per second
Contingency = 8 bytes per second